

## Mechanistic Basis of OXA-48-like $\beta$ -Lactamases' Hydrolysis of Carbapenems

Vlatko Stojanoski, Liya Hu, Banumathi Sankaran, Feng Wang, Peng Tao, B. V. Venkataram Prasad, and Timothy Palzkill\*



Cite This: ACS Infect. Dis. 2021, 7, 445–460



Read Online

ACCESS |

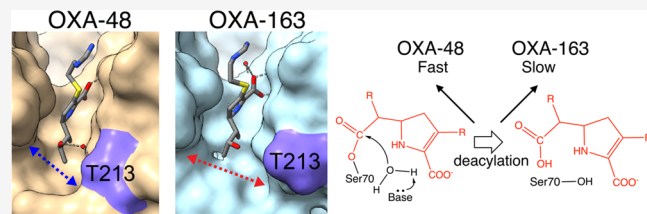
Metrics & More

Article Recommendations

Supporting Information

**ABSTRACT:** Carbapenem-hydrolyzing class D  $\beta$ -lactamases (CHDLs) are an important source of resistance to these last resort  $\beta$ -lactam antibiotics. OXA-48 is a member of a group of CHDLs named OXA-48-like enzymes. On the basis of sequence similarity, OXA-163 can be classified as an OXA-48-like enzyme, but it has altered substrate specificity. Compared to OXA-48, it shows impaired activity for carbapenems but displays an enhanced hydrolysis of oxyimino-cephalosporins. Here, we address the mechanistic and structural basis for carbapenem hydrolysis by OXA-48-like enzymes. Pre-steady-state kinetic analysis indicates that the rate-limiting step for OXA-48 and OXA-163 hydrolysis of carbapenems is deacylation and that the greatly reduced carbapenemase activity of OXA-163 compared to that of OXA-48 is due entirely to a slower deacylation reaction. Furthermore, our structural data indicate that the positioning of the  $\beta 5\text{-}\beta 6$  loop is necessary for carbapenem hydrolysis by OXA-48. A major difference between the OXA-48 and OXA-163 complexes with carbapenems is that the 214-RIEP-217 deletion in OXA-163 creates a large opening in the active site that is absent in the OXA-48/carbapenem structures. We propose that the larger active site results in less constraint on the conformation of the  $6\alpha$ -hydroxyethyl group in the acyl-enzyme. The acyl-enzyme intermediate assumes multiple conformations, most of which are incompatible with rapid deacylation. Consistent with this hypothesis, molecular dynamics simulations indicate that the most stable complex is formed between OXA-48 and imipenem, which correlates with the OXA-48 hydrolysis of imipenem being the fastest observed. Furthermore, the OXA-163 complexes with imipenem and meropenem are the least stable and show significant conformational fluctuations, which correlates with the slow hydrolysis of these substrates.

**KEYWORDS:** antibiotic resistance, carbapenems, serine  $\beta$ -lactamases, OXA-enzymes, carbapenemases, OXA-48-like enzymes



### INTRODUCTION

Antibiotic resistance is a worldwide problem that is growing at an alarming rate.<sup>1–3</sup> An increasing number of bacterial infections acquired in hospital settings are caused by carbapenem-resistant *Enterobacteriaceae* (CRE) pathogens.<sup>4–6</sup> The major causative agents of CRE infections are bacterial species belonging to the Gram-negative bacilli *Klebsiella*, with *Klebsiella pneumoniae* representing 80% of these infections.<sup>7–10</sup> Resistance to carbapenems is a concern in that these drugs have a broad spectrum of activity, high potency, and are used as last-resort  $\beta$ -lactam antibiotics for infections with pathogens resistant to earlier-generation antibiotics.<sup>11–13</sup>

*Klebsiella pneumoniae* frequently become resistant to carbapenem antibiotics by acquiring plasmid-encoded  $\beta$ -lactamases named carbapenemases.<sup>14,15</sup>  $\beta$ -Lactamases are grouped into four classes (A–D) based on their primary amino acid sequence homology. Classes A, C, and D are serine hydrolases, and class B consists of zinc metallo-enzymes.<sup>16,17</sup> Carbapenemases found in *K. pneumoniae* belong to either metallo- (class B) or serine  $\beta$ -lactamase (classes A and D) classes.<sup>18</sup> The three most frequently encountered carbapene-

mases in clinics worldwide are KPC (class A), OXA-48 (class D), and NDM (class B).<sup>18–20</sup>

OXA-48 was first isolated more than a decade ago from a nosocomial infection with *K. pneumoniae* in Turkey and since then has been disseminated worldwide.<sup>21</sup> OXA-48 is a carbapenem-hydrolyzing, class D  $\beta$ -lactamase (CHDL). Among all class D enzymes, it has the highest catalytic efficiency ( $k_{cat}/K_m$ ) for the hydrolysis of the carbapenem imipenem.<sup>19,22</sup> OXA-48 is a member of a subgroup of class D enzymes termed OXA-48-like enzymes, which includes 12 enzymes differing from OXA-48 by one to five amino acids.<sup>23,24</sup> Most enzymes in the OXA-48-like group have very similar carbapenemase profiles.<sup>19,24</sup> Exceptions to this are OXA-163, OXA-247, and OXA-405, which are grouped with OXA-48-like enzymes by sequence homology yet display poor

Received: November 16, 2020

Published: January 25, 2021



carbapenemase activity.<sup>23–25</sup> Previous reports show that OXA-48 and OXA-163 also have very different catalytic efficiencies for the hydrolysis of other  $\beta$ -lactam antibiotics such as oxyimino-cephalosporins.<sup>24,26</sup> OXA-163, similar to OXA-48, was isolated in the clinic from an infection of *K. pneumoniae*, but it differs from OXA-48 by one substitution, S212D, and a four amino acid deletion, 214-RIEP-217.<sup>26</sup> The sequence changes in OXA-163 eliminate the bottom boundary of the active site, causing an expansion of the active-site cavity<sup>27</sup> (Figure 1).

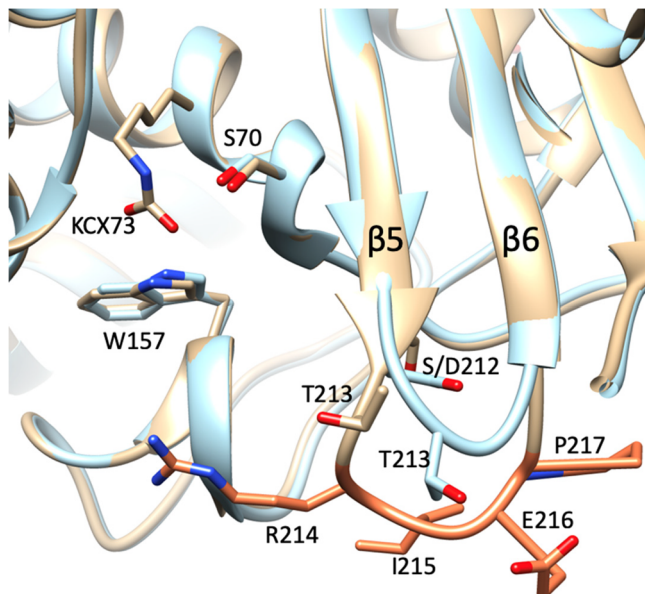


**Figure 1.** Overlay of OXA-48 (tan) and OXA-163 (light blue) outlining the active site cavity. In the center is the S70 nucleophile, and to the left of the serine is the N-carboxylated K73 general base, which is coordinated in part by W157. Represented by an orange stick model are the four residues deleted in OXA-163. The important elements outlining the active site are labeled. The active site is confined between the  $\beta$ 5 strand on the right and the bottom in OXA-48 by R214. In OXA-163, the absence of R214 extends the active site by eliminating the bottom boundary.

Class D  $\beta$ -lactamases such as OXA-48 are serine hydrolases with a mechanism similar to that of serine proteases. After the formation of the enzyme–substrate complex (ES), the active-site serine attacks and forms a covalent acyl-enzyme intermediate (EAc).<sup>28</sup> Subsequent activation of a water molecule and hydrolysis of the acyl-enzyme generates the hydrolyzed product (P) (Scheme 1), which is inactive as an antibiotic. In class D enzymes, the deacylation water is activated by a carboxylated lysine.<sup>29</sup>

Unlike the OXA-48-like enzymes, most class D  $\beta$ -lactamases are inhibited by carbapenems via the formation of a long-lived, covalent acyl-enzyme complex.<sup>12</sup> For these enzymes, nucleophilic attack by the catalytic Ser70 to form the acyl-enzyme occurs rapidly, but deacylation by water to the hydrolyzed

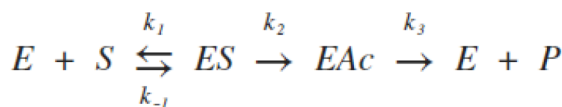
product occurs very slowly. Carbapenems are thought to be poor substrates for  $\beta$ -lactamases due to the presence of the pyrroline ring adjacent to the  $\beta$ -lactam ring as well as the small R1 6 $\alpha$ -hydroxyethyl moiety.<sup>30–32</sup> Several mechanisms have been proposed to explain the poor hydrolysis of carbapenems by serine active-site  $\beta$ -lactamases. First, the pyrroline ring can undergo tautomerization upon acylation by the catalytic serine, which produces two isomers,  $\Delta^1$  and  $\Delta^2$  (Figure S1). The  $\Delta^2$  isomer has been suggested to be more favorable for subsequent deacylation and hydrolysis.<sup>33,34</sup> Second, the 6 $\alpha$ -hydroxyethyl group forms a hydrogen bond with the deacylating water and reduces its nucleophilicity, thereby slowing the deacylation rate.<sup>30</sup> In contrast, the SFC-1 class A carbapenemase constrains the position of the hydroxyethyl group away from the water, which is suggested to enhance the nucleophilicity of the water, leading to a faster deacylation rate.<sup>32</sup> Finally, structures of the noncarbapenemase TEM-1 and SHV-1 class A  $\beta$ -lactamases acylated by imipenem and meropenem, respectively, reveal a conformational change in the acylated substrate whereby the carbonyl oxygen of the  $\beta$ -lactam ring is no longer in the oxyanion hole, thereby blocking the deacylation reaction.<sup>30,31</sup>

In class D  $\beta$ -lactamases, additional factors interfere with carbapenem hydrolysis. The 6 $\alpha$ -hydroxyethyl group obstructs access for a water molecule to be activated by the carboxylated lysine and attack the carbonyl carbon of the acyl-enzyme.<sup>35,36</sup> To explain how a nucleophilic water gains access to the acyl enzyme in OXA-23 and OXA-143 it has been proposed that movement of either a conserved active site leucine or valine opens a channel for the water molecule to reach the catalytic lysine to promote deacylation.<sup>35</sup> It has also been suggested, on the basis of X-ray structures and molecular dynamics simulations, that the rotation of a carbapenem in the active site of OXA-48 may allow access of a water molecule to a position consistent with deacylation.<sup>22,36</sup>

Because of the high clinical relevance, there have been several recent structural studies on the mechanism of carbapenem hydrolysis by OXA-48.<sup>36–38</sup> However, the acylation and deacylation rate constants for carbapenem hydrolysis by OXA-48 are not known, and the mechanism behind the decrease in carbapenem hydrolysis by the OXA-163 enzyme has not been addressed. To investigate the mechanism of carbapenem hydrolysis mediated by OXA-48 and OXA-163, pre-steady-state kinetic studies were performed for imipenem and meropenem, revealing that the deacylation of the acyl-enzyme intermediate is the rate-limiting step for both enzymes for both substrates. However, compared to OXA-48, OXA-163 has a greatly decreased deacylation rate that results in the slow hydrolysis of carbapenems.

To gain further insight into the structural basis of the different substrate profiles of OXA-48 and OXA-163 and, more generally, the basis of the high carbapenemase activity of OXA-48-like enzymes, we determined the structures of the acyl-enzyme intermediates of these enzymes with imipenem and meropenem. The structures show in all cases that the acylated carbapenem is in the  $\Delta^2$  tautomeric form and that the carbonyl oxygen originating from the  $\beta$ -lactam ring is positioned in the oxyanion hole. These findings are consistent with efficient deacylation. Thus, tautomerization and the occupancy of the oxyanion hole cannot explain the differences in catalysis/specification between OXA-48 and OXA-163. Furthermore, the hydroxyl group from the 6 $\alpha$ -hydroxyethyl moiety is directed away from the carboxylated lysine and deacylation water for both carbapenems in the OXA-48 and OXA-163 structures,

### Scheme 1



suggesting that it does not play a role in the slow deacylation of carbapenems by these enzymes. A major difference between the OXA-48 and OXA-163 complexes with carbapenems is the 214-RIEP-217 deletion in OXA-163, which creates a large opening in the active site that is absent in the OXA-48/carbapenem structures. We propose that the larger active site results in less constraint on the conformation of the  $6\alpha$ -hydroxyethyl group in the acyl-enzyme, which allows the intermediate to assume multiple nonproductive conformations that would slow deacylation. Finally, molecular dynamics simulation studies of complexes of OXA-48 and OXA-163 with imipenem and meropenem indicate that the most stable complex is formed between OXA-48 and imipenem, which correlates with the OXA-48 hydrolysis of imipenem being the fastest observed. The OXA-163 complexes with imipenem and meropenem are also less stable and show significant conformational fluctuations compared to complexes with OXA-48, which correlates with the slow hydrolysis of these substrates by OXA-163.

## RESULTS

**Carbapenem Turnover Is Reduced in OXA-163 versus OXA-48.** Noncarbapenemase class D  $\beta$ -lactamases hydrolyze carbapenems poorly due to a very slow deacylation rate. OXA-48 hydrolyzes carbapenems more rapidly, but the rate-limiting step of this reaction is not known. OXA-163 is an OXA-48-like variant that hydrolyzes carbapenems slowly, but the kinetic basis for the slower rate is not known.

To examine the kinetics of carbapenem hydrolysis, steady-state kinetics experiments were performed with imipenem and meropenem as substrates (Table 1). OXA-48 displays a 28-

imipenem hydrolysis by OXA-48 is 45-fold higher than that for meropenem. In the  $\beta$ -lactamase kinetic scheme,  $k_{cat}/K_M$  reflects the rates up to the formation of the acyl-enzyme and therefore indicates an increased binding affinity ( $K_D$ ) and/or a faster acylation rate ( $k_2$ ) for imipenem versus meropenem for OXA-48. Finally, the  $K_M$  values for both imipenem and meropenem hydrolysis by OXA-48 are very low (<5  $\mu$ M). It was not possible to accurately determine the values because of the low substrate concentrations involved (Table 1).  $K_M$  is a complex term in the  $\beta$ -lactamase kinetic scheme and does not necessarily reflect the substrate binding affinity in that a strongly limiting deacylation rate ( $k_3$ ) can also lead to low  $K_M$  values.<sup>41,42</sup>

OXA-48, like most other family members, is a good catalyst for carbapenem hydrolysis, although imipenem is a 30-fold better substrate than meropenem. In comparison to OXA-48, OXA-163 has lost considerable activity (about a 500-fold decrease in  $k_{cat}$ ) for imipenem hydrolysis and has somewhat lower activity against meropenem (5-fold) (Table 1). This result is opposite to the characteristic CHBL profile that is observed for OXA-48.<sup>27</sup> Because  $k_{cat}$  is reduced,  $k_2$  and/or  $k_3$  must be slower for imipenem and meropenem catalysis by OXA-163 compared to OXA-48. Therefore, the four amino acid deletions and S212D substitution present in OXA-163 relative to OXA-48 result in a decrease in carbapenem turnover, particularly for imipenem.

The  $k_{cat}/K_M$  value for imipenem hydrolysis by OXA-163 is nearly 1000-fold lower than that for OXA-48, while that for meropenem is 5-fold lower than that for OXA-48. This result indicates that the substrate binding affinity ( $K_D$ ) and/or the acylation rate are reduced by the four amino acid deletion and S212D substitution present in OXA-163 relative to OXA-48. As with OXA-48, the  $K_M$  values for carbapenem hydrolysis by OXA-163 are very low with both imipenem and meropenem as substrates (Table 1). Consequently, it was not possible to directly determine the  $K_M$  because of the low substrate concentrations that would be required. As noted above, a low  $K_M$  does not necessarily reflect tight substrate binding as rate-limiting deacylation can lead to  $K_M$  values below the  $K_D$  for the substrate.

**Carbapenem Deacylation Is Rate-Limiting for OXA-48 and Strongly Rate-Limiting for OXA-163.** The steady-state kinetic parameters for both imipenem and meropenem hydrolysis indicate a large decrease in  $k_{cat}$  for OXA-163 compared to that for OXA-48 (Table 1). Since the  $\beta$ -lactam hydrolysis reaction consists of two distinct steps (acylation and deacylation) as outlined in Scheme 1, the  $k_{cat}$  value is constrained by the rate-limiting step, which in the case of serine  $\beta$ -lactamases may be acylation, deacylation, or both if the rates are similar.<sup>41,43,44</sup> The steady-state kinetic data do not allow the determination of the rate-limiting steps in carbapenem hydrolysis for either enzyme. Consequently, the individual acylation ( $k_2$ ) and deacylation ( $k_3$ ) rate constants were determined experimentally for both enzymes using the pre-steady-state kinetics and recovery of enzymatic activity assays, respectively.<sup>45,46</sup>

The acylation rate constants for imipenem and meropenem were determined by stopped-flow kinetics under single-turnover conditions with excess enzyme<sup>45,47</sup> (Table 1, Figure 2). OXA-48 and OXA-163 were found to have similar acylation rate constants (less than a 3-fold difference) for both carbapenems. In the case of imipenem, the  $k_2$  values were much larger than the corresponding  $k_{cat}$  values (30-fold for

**Table 1. Kinetic Parameters of OXA-48 and OXA-163**

enzyme	substrate	
	imipenem	meropenem
OXA-48		
$k_{cat}$ ( $s^{-1}$ )	$2.8 \pm 0.2$	$0.1 \pm 0.01$
$K_m$ ( $\mu$ M)	$\leq 3.0 \pm 0.6$	$\leq 5.0 \pm 1.5$
$k_{cat}/K_m$ ( $M^{-1} s^{-1}$ )	$\geq 9.1 \times 10^5$	$\geq 2.0 \times 10^4$
$k_2$ ( $s^{-1}$ )	$86 \pm 12$	$300 \pm 28$
$k_3$ ( $s^{-1}$ )	$3.0^{a}$ $\pm 1.1$	$0.15 \pm 0.01$
$K_s'$ ( $\mu$ M)	$98 \pm 32$	$129 \pm 31$
OXA-163		
$k_{cat}$ ( $s^{-1}$ )	$0.005 \pm 0.001$	$0.022 \pm 0.002$
$K_m$ ( $\mu$ M)	$\leq 3.8 \pm 1$	$5.6 \pm 0.5$
$k_{cat}/K_m$ ( $M^{-1} s^{-1}$ )	$\geq 1.3 \times 10^3$	$3.9 \times 10^3$
$k_2$ ( $s^{-1}$ )	$250 \pm 19$	$95 \pm 7$
$k_3$ ( $s^{-1}$ )	$0.011 \pm 0.005$	$0.031 \pm 0.011$
$K_s'$ ( $\mu$ M)	$92 \pm 22$	$21 \pm 5$

<sup>a</sup>This rate constant was determined using eq 4. The error in the calculated  $k_3$  value was determined by propagating the error in  $k_{cat}$  and  $k_2$  (Materials and Methods).

fold-higher turnover rate ( $k_{cat}$ ) for the hydrolysis of imipenem compared to the rate for the hydrolysis of meropenem, consistent with the observation that several CHDL enzymes hydrolyze imipenem faster than meropenem.<sup>24,27,39,40</sup> In the  $\beta$ -lactamase kinetic scheme,  $k_{cat}$  reflects the magnitude and relationship between the acylation ( $k_2$ ) and deacylation ( $k_3$ ) rates;<sup>41,42</sup> therefore, the 28-fold-increased turnover of imipenem reflects higher  $k_2$  and/or  $k_3$  values compared to the values for meropenem. Similarly, the  $k_{cat}/K_M$  value for

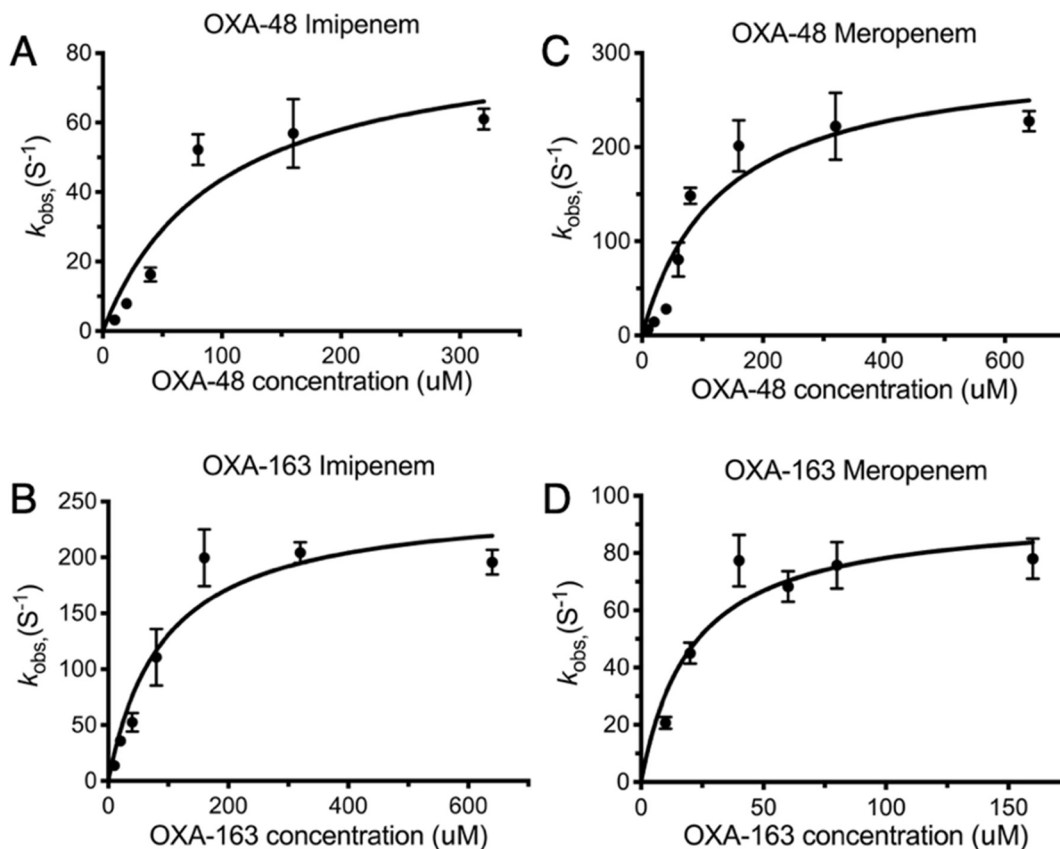


**Figure 2.** Determination of  $k_2$  based on fits of the apparent constants ( $k_{obs}$ ) obtained using single-turnover kinetics for OXA-48 and OXA-163 with imipenem and meropenem. (A and C)  $k_{obs}$  values of OXA-48 for imipenem and meropenem, respectively. (B and D) Determination of  $k_2$  based on fits of  $k_{obs}$  values of OXA-163 for imipenem and meropenem, respectively. Acylation constants were determined using eq 2.

OXA-48 and 50 000-fold for OXA-163), indicating that acylation is not the rate-limiting step for imipenem hydrolysis by either enzyme. The acylation rate constants for meropenem hydrolysis were also much higher than the corresponding  $k_{cat}$  values (3000-fold for OXA-48 and 4300-fold for OXA-163), indicating that acylation is not rate-limiting, even with a poorer substrate. Overall, the acylation rate constants for imipenem and meropenem hydrolysis by OXA-48 and OXA-163 indicate that both enzymes acylate these carbapenem substrates relatively rapidly and at similar rates.

To test the hypothesis that deacylation is rate-limiting for the hydrolysis of imipenem and meropenem by OXA-48 and OXA-163, the deacylation rate constants ( $k_3$ ) were determined directly using the enzyme reactivation method.<sup>46</sup> Progress curves of hydrolysis of colorimetric substrate nitrocefin revealed the reactivation rates of OXA-48 and OXA-163 after incubation with imipenem and meropenem (Figure 3, Table 1). In all cases, the deacylation rate constants ( $k_3$ ) were much lower than the rate constants observed for acylation and were comparable to the corresponding  $k_{cat}$  values (Table 1). This confirms that deacylation is the rate-limiting step for carbapenem hydrolysis by both OXA-48 and OXA-163. The deacylation rate of imipenem by OXA-48 could not be measured accurately by the reactivation method because of fast recovery due to a relatively high  $k_{cat}$  value (Figure 3, Table 1). As a result, the  $k_3$  for OXA-48 with imipenem was obtained with eq 4 using the experimentally determined  $k_{cat}$  and  $k_2$  values. This calculation yields a  $k_3$  of  $3.0\text{ s}^{-1}$  for OXA-48 with imipenem, which is almost identical to the  $k_{cat}$  of  $2.8\text{ s}^{-1}$ ,

indicating that the rate-limiting step is deacylation. The OXA-48 deacylation rate constant for imipenem was 20-fold higher than that for meropenem. Thus, meropenem is turned over more slowly by OXA-48 compared to imipenem due to slower deacylation. Moreover, the  $k_3$  values of OXA-48 for imipenem and meropenem are higher than the  $k_3$  values of OXA-163 by 270-fold and 5-fold, respectively. Therefore, OXA-163 is a poor carbapenemase compared to OXA-48 because of slower deacylation rates.

In summary, the kinetics results indicate that the rate-limiting step for the hydrolysis of both imipenem and meropenem by the OXA-48 carbapenemase is deacylation. In addition, the slower hydrolysis of meropenem versus imipenem by OXA-48 can be attributed to the much slower deacylation of meropenem. Finally, the S212D substitution and 214-RIEP-217 deletion in OXA-163 relative to OXA-48 further perturb the deacylation step, leading to a large decrease in the turnover rate compared to the turnover rate for OXA-48. This is especially pronounced in the case of imipenem. The deacylation rate constant for meropenem is less affected by the structural changes between OXA-48 and OXA-163.

**X-ray Structures of the OXA-48 K73A Mutant Reveal Similar Conformations of Carbapenems in the Active Site.** Having determined that deacylation is rate-limiting for carbapenem hydrolysis by both OXA-48 and OXA-163, we next determined the X-ray structures of deacylation-deficient K73A mutants of OXA-48 and OXA-163 in complex with imipenem and meropenem to investigate the structural differences that contribute to the observed deacylation rates.

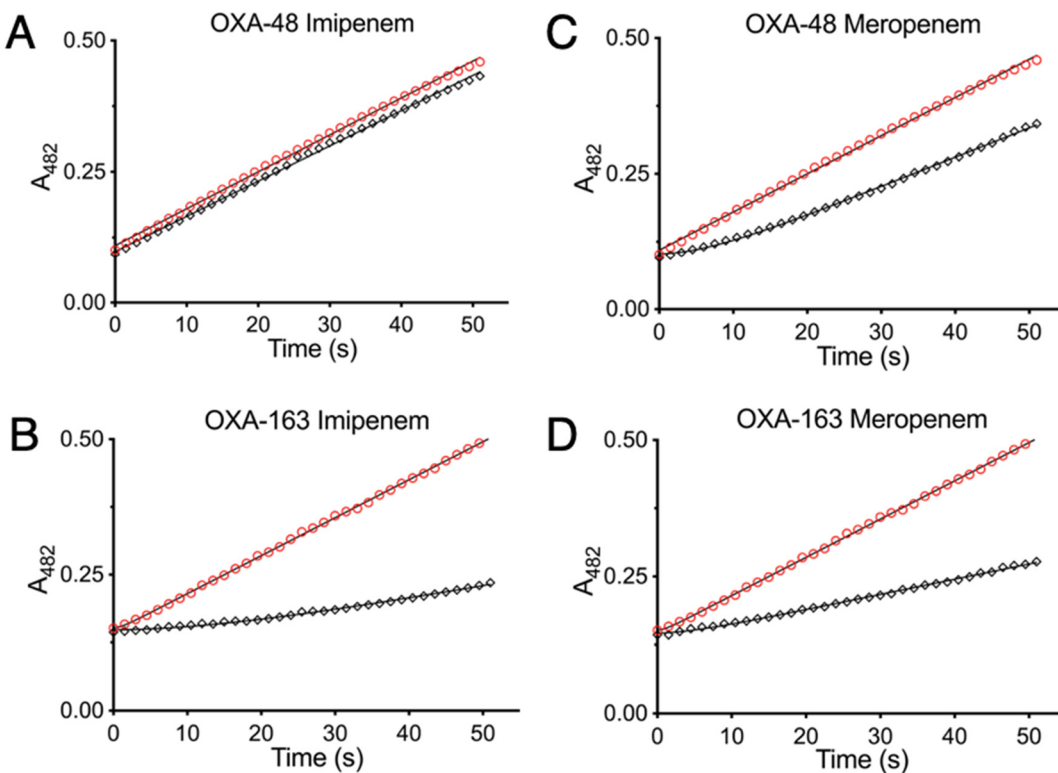


**Figure 3.** Reactivation of OXA-48 and OXA-163 after incubation with imipenem and meropenem. (A and C) Progress curves and fits of OXA-48 nitrocefin hydrolysis after incubation with imipenem and meropenem. (B and D) Progress curves and fits of OXA-163 nitrocefin hydrolysis after incubation with imipenem and meropenem, respectively. The red circles show the control condition of nitrocefin hydrolysis in the absence of incubation with carbapenem. The black diamonds show the experimental condition of nitrocefin hydrolysis after incubation with carbapenem. The black lines are the fits of the data to eq 3 (Materials and Methods).

K73A mutants were used to prevent substrate turnover since the wild-type enzymes hydrolyze the  $\beta$ -lactam ring and release the inactivated product. Previously, K73A mutants have been used successfully to determine the structure of the acyl-enzyme complex of OXA-enzymes with  $\beta$ -lactam antibiotics.<sup>48</sup>

The crystal structure of OXA-48 K73A bound to imipenem was determined at 2.3 Å resolution (Table 2). The structure crystallized with two molecules in the asymmetric unit in the P2<sub>2</sub>1<sub>2</sub>1 space group. Strong residual electron density in the F<sub>o</sub> – F<sub>c</sub> simulated-annealing-omitted difference maps indicated the presence of imipenem attached to the O $\gamma$  of Ser70 in both chains. The two chains in the asymmetric unit are superimposable, and the covalently attached imipenem also shows a very similar structure with minor differences in the extended, flexible C2 substituent (Figure S2). Hydrogen bonds constituting the oxyanion hole occur between the –NH main chain atoms of Ser70 and Tyr211 and the C7 acyl-carbonyl oxygen of imipenem (Figures 4A and 5). Also, the C3 carboxyl group of imipenem interacts via hydrogen bonds with the side chains of Thr209 and Arg250 (Figures 4A and 5). Previous structures of OXA-48 with acylated imipenem have revealed two tautomers of the pyrroline ring.<sup>36,38</sup> In the  $\Delta^1$  tautomer, the C2 atom of the pyrroline ring is sp<sup>3</sup> hybridized, while the  $\Delta^2$  state has C2 in a planar configuration, indicating sp<sup>2</sup> hybridization. Both chains of the OXA-48 K73A/imipenem structure display the  $\Delta^2$  tautomeric state (Figure 4A). The hydroxyethyl group of imipenem is in a similar position and conformation as observed in previous OXA-48 acyl-enzyme complexes. The hydroxyl group is oriented away from residue 73, and the methyl group is in a pocket defined by Val120,

Leu158, and Ala69<sup>36,38</sup> (Figures 4A and 6A,B). The orientation of the hydroxyl group away from the pocket that would contain the carboxylated Lys73 general base and the deacylating water indicates that it would not inactivate these groups as it is suggested to do in noncarbapenemase enzymes.<sup>30,32</sup> This finding is consistent with the relatively fast deacylation rate for imipenem (Table 1). A notable difference between our OXA-48 K73A/imipenem structure and previous structures is the conformation of Ser118 (Figures 4A and 6A,B). In previous structures, the Ser118 rotamer has a  $\chi_1 \approx -150^\circ$  value while the K73A/imipenem structure has a Ser118 rotamer with  $\chi_1 \approx -60^\circ$  (Figures 4A and 6A,B). This is likely due to the K73A substitution, which eliminates a hydrogen bond between Lys73 and Ser118 that stabilizes the  $\chi_1 \approx -150^\circ$  conformation.

The OXA-48 K73A/meropenem acyl-enzyme structure was determined at 2.0 Å resolution (Figure 4C and Table 2). This structure is also very similar to previously determined OXA-48/meropenem acyl-enzyme structures with the meropenem carbonyl oxygen in the oxyanion hole, the C3 carboxylate making hydrogen bonds to Thr209 and Arg250, and the hydroxyethyl group oriented as in the OXA-48 K73A/imipenem structure with the methyl group in the hydrophobic pocket formed by Ala69, Val120, and Leu158 and the hydroxyl oriented away from Lys73, where it would not interfere with the general base or deacylation water (Figures 4C, 5, and 6C,D). While this orientation of the hydroxyethyl group is consistent with meropenem hydrolysis, it does not offer a ready explanation for why meropenem is deacylated at a slower rate than imipenem. As with the imipenem structure, the effect

**Table 2.** Crystal Data Collection and Structure Refinement Statistics

PDB ID	OXA48 K73A/imipenem 7KH9	OXA48 K73A/meropenem 7KHZ	OXA163 K73A/imipenem 7KHZ	OXA163 K73A/meropenem 7KHY
Data Collection				
wavelength (Å)	1.54	0.997	0.997	0.997
resolution range (Å)	26.87–2.29 (2.37–2.29)	34.24–2.0 (2.04–2.0)	44.16–2.04 (2.11–2.04)	43.9–1.84 (1.94–1.84)
space group	P22 <sub>1</sub> 2 <sub>1</sub>	P22 <sub>1</sub> 2 <sub>1</sub>	C222 <sub>1</sub>	C222 <sub>1</sub>
Unit Cell				
<i>a, b, c</i> (Å)	44.7, 104.8, 125.1	44.3, 105.5, 125.7	44.4, 88.3, 125.4	44.3, 87.8, 125.0
$\alpha, \beta, \gamma$ (deg)	90, 90, 90	90, 90, 90	90, 90, 90	90, 90, 90
total reflections	53 411 (5218)	334 567 (15 962)	31 234 (3027)	42 948 (4223)
unique reflections	27 105 (2650)	40 232 (1925)	15 808 (1538)	21 551 (2118)
multiplicity	2.0 (2.0)	8.3 (8.3)	2.0 (2.0)	6.7 (6.9)
completeness (%)	99.4 (99.1)	99.1 (98.0)	98.0 (97.2)	99.6 (99.6)
mean <i>I</i> / <i>sigma</i> ( <i>I</i> )	10.73 (2.25)	11.02 (1.20)	11.63 (2.10)	15.88 (4.25)
Wilson <i>B</i> factor	27.8	22.2	20.3	19.80
<i>R</i> merge (%)	5.1 (25.2)	9.4 (66.6)	5.0 (26.0)	7.7 (39.4)
Refinement				
<i>R</i> <sub>work</sub> (%)/ <i>R</i> <sub>free</sub> (%)	18.3/22.7	20.8/23.6	18.6/23.6	19.2/24.0
total numbers of atoms	4318	4283	2098	2120
protein residues	484	484	237	237
RMS (bonds)	0.003	0.005	0.003	0.004
RMS (angles)	0.768	0.615	0.645	0.684
Ramachandran analysis				
favorable (%)	97.7	97.9	98.3	98.7
allowed (%)	2.3	2.1	1.7	1.3
outliers (%)	0	0	0	0
average <i>B</i> factor	28.1	29.0	24.5	23.4
protein	27.7	28.5	23.8	22.6
ligands	39.0	41.2	44.9	38.2
solvent	32.2	34.6	31.2	30.2

of the K73A mutation is a change in the rotamer distribution of Ser118. Finally, the weak density and high *B* factors of the C2 substituent suggests the meropenem C2 substituent is flexible in the structure.

**X-ray Structures of the OXA-163 K73A Mutant Reveal Multiple Conformations of Carbapenems in the Active Site.** As noted above, the OXA-163 enzyme contains the S212D substitution and 214-RIEP-217 deletion compared to OXA-48, which results in an increased rate of oxyiminocephalosporin hydrolysis but a drastically decreased rate of carbapenem hydrolysis due to slow deacylation.<sup>27</sup> To understand the basis for the decreased carbapenem hydrolysis rate, we determined the acyl-enzyme structures of an OXA-163 K73A mutant in complex with imipenem and meropenem. The OXA-163 K73A/imipenem complex crystallized with one molecule in the asymmetric unit in the C222<sub>1</sub> space group, and the structure was determined at 2.0 Å resolution (Figure 4B and Table 2). As with the OXA-48 K73A/imipenem structure, the imipenem carbonyl oxygen is in the oxyanion hole, and the C3 carboxylate group makes hydrogen bonds to the side chains of Thr209 and Arg250 (Figures 4A,B and 5). In addition, the C2 group is planar with the ring, indicating sp<sup>2</sup> hybridization consistent with the Δ<sup>2</sup> tautomer. A further similarity is the presence of the Ser118 χ<sub>1</sub> ≈ −60° rotamer conformation, presumably due to the K73A substitution (Figure 4B and Figure 6A,B). Finally, the hydroxyethyl group is positioned as in the OXA-48 K73A/imipenem structure with the hydroxyl oriented away from Lys73 where it would not interfere with the general base or deacylation water.

There are also differences in the OXA-163 K73A/imipenem structure compared to the OXA-48 K73A/imipenem structure. The major difference is that the 214-RIEP-217 deletion creates a large opening in the active site that is absent in the OXA-48 K73A/imipenem structure (Figures 4A,B and 7A,B). For example, Thr213 is displaced by 2.33 Å, which leads to the loss of interactions with the 6α-hydroxyethyl group, suggesting that the larger active site might place fewer constraints on the conformation of the 6α-hydroxyethyl group (Figure 7B and Table 1).

The OXA-163 K73A meropenem-bound acyl-enzyme structure was determined at 1.9 Å resolution in the same space group and asymmetric unit specification as for the imipenem structure (Table 2). Meropenem is hydrolyzed by OXA-48 with a 20-fold-lower *k*<sub>cat</sub> than for imipenem due to slower deacylation (Table 1). OXA-163, however, hydrolyzes meropenem with a *k*<sub>cat</sub> that is 5-fold slower than that for OXA-48 due to even slower deacylation. As with the OXA-163/imipenem structure, the OXA-163 K73A/meropenem structure showed residual electron density extending from the Oγ of Ser70, indicative of covalently bound meropenem (Figure 4D). Many of the polar and hydrophobic interactions of meropenem with the OXA-163 enzyme are identical to the imipenem interactions (Figure 4B,D and Figure 5). Specifically, the formation of the oxyanion hole by the −NH of Ser70 and the −NH of Tyr211 and the coordination of the C3 carboxyl by Thr209 and Arg250 are similar (Figure 5). The pyrrolidine ring of meropenem also demonstrated a planar-like appearance indicating sp<sup>2</sup> hybridization of the C2 carbon and the presence of the Δ<sup>2</sup> tautomer. The R2 group of meropenem shows

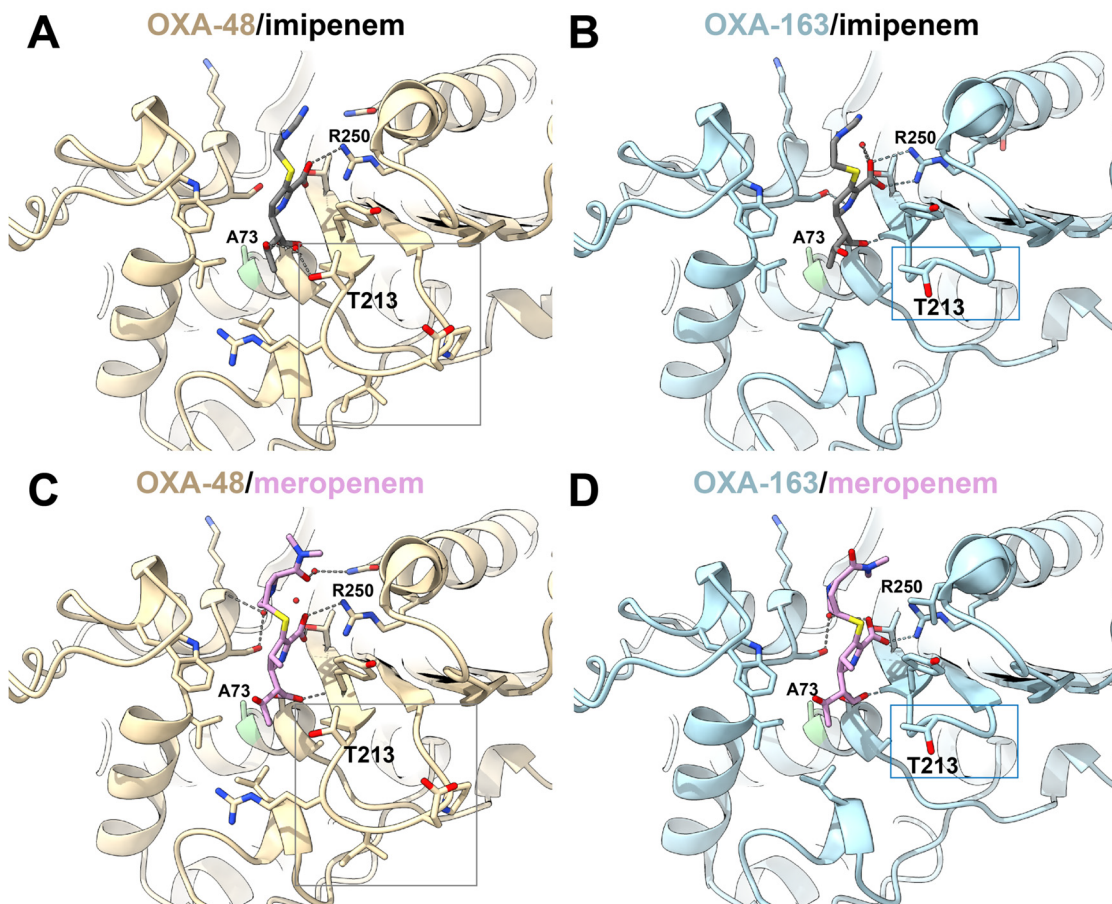


**Figure 4.** Schematic of the structures of the OXA-48 K73A and OXA-163 K73A acyl-enzyme complexes with imipenem and meropenem. (A) Active-site region of the OXA-48 K73A enzyme with Ser70 forming a covalent acyl-enzyme with imipenem. The  $\beta_5\text{-}\beta_6$  loop containing Thr213 that constrains the size of the active site is indicated in the boxed region. Hydrogen bonds are shown as dotted black lines. Carbon atoms are shown in tan, oxygen in red, nitrogen in blue, and sulfur in yellow. Imipenem carbon atoms are shown in gray. (B) Active-site region of the OXA-163 K73A enzyme with Ser70 forming a covalent acyl-enzyme with imipenem. The active site is more open than OXA-48 due to the reduced size of the  $\beta_5\text{-}\beta_6$  loop containing Thr213 (boxed region). Carbon atoms are shown in light blue. (C) Active-site region of the OXA-48 K73A enzyme with Ser70 forming a covalent acyl-enzyme with meropenem. Meropenem carbon atoms are shown in pink. (D) Active-site region of the OXA-163 K73A enzyme with Ser70 forming a covalent acyl-enzyme with meropenem. Meropenem carbon atoms are shown in pink.

flexibility as indicated by weaker electron density and higher *B* factors (Figure 4D). Finally, as with the OXA-48 K73A/imipenem, OXA-48 K73A/meropenem, and OXA-163 K73A/imipenem structures, the hydroxyethyl group is bound with the hydroxyl oriented away from Lys73 where it would not interfere with the general base or deacylation water.

In all of the OXA-48 K73A and OXA-163 K73A structures, the cavity formerly occupied by the carbamylated Lys73 is occupied by a mixture of water and chloride ions. For the OXA-48 K73A/imipenem structure, the space is occupied by a water and a chloride ion in chains A and B (Figure S3). In the OXA-48 K73A/meropenem structure, the cavity is occupied by two water molecules in chain A and three waters in chain B (Figure S3). In the OXA-163 K73A/imipenem structure, the cavity is occupied by two waters, and in the OXA-163 K73A/meropenem structure, the cavity is occupied by a water and a chloride ion. The waters in these structures are not positioned to effectively attack the carbonyl carbon of the acyl-enzyme for the deacylation reaction (Figure S3).

The structural results suggest that the slow rate of deacylation of carbapenems by OXA-163 is not due to the hydroxyl oxygen of the  $6\alpha$ -hydroxyethyl group hydrogen bonding to the carbamylated Lys73 or deacylating water to

lower basicity or nucleophilicity, respectively. Alternatively, it is possible that the slow deacylation of both imipenem and meropenem by OXA-163 is due to a larger active site that does not adequately constrain the carbapenem acyl-enzyme, leading to conformational heterogeneity (Figure 7B,D). The existence of multiple inactive conformations of the acyl-enzyme could account for the slow deacylation of both carbapenems.

**Molecular Dynamics Simulations Reveal That OXA-163 Carbapenem Complexes Are Unstable in the Active Site.** The basis for the different rates of acyl-enzyme hydrolysis between imipenem and meropenem for OXA-48 and OXA-163 was evaluated using molecular dynamics simulations. For this purpose, the structures of the imipenem and meropenem acyl-enzymes of the OXA-48 K73A and OXA-163 K73A mutants were used to construct models of the enzymes with Lys73 restored and carboxylated and with the substrate bound in the active site. The modified structures were subjected to energy minimization with steepest descent and ABNR minimization steps. Subsequently, the minimized simulation systems were subjected to 40 ps equilibrium MD simulations while the temperature was gradually increased from 100 to 300 K. The production MD simulations were carried out as NTP ensemble MD simulations at 300 K and 1 atm for 100 ns (*Methods*).

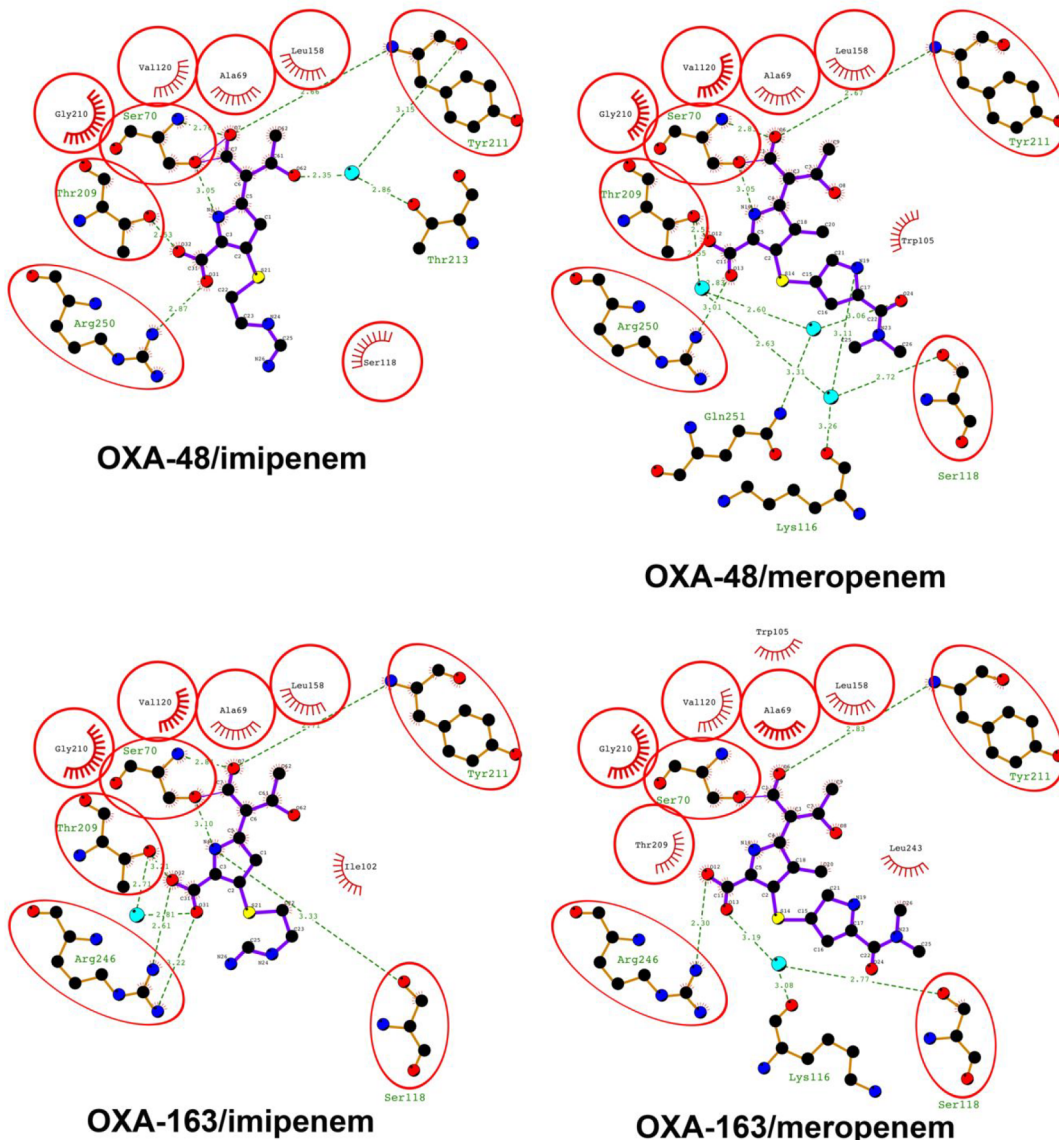


**Figure 5.** Ligplot diagram showing the hydrogen bonding and hydrophobic interactions between OXA-48 and OXA-163 with imipenem and meropenem.

The root-mean-square deviation (RMSD) distributions of heavy atoms of the entire OXA-48 and OXA-163 enzymes plus substrate as well as the active-site region plus the substrate were calculated. For this purpose, residues including Ser70, Kcx73, Ser118, Trp157, and Lys208 were defined as the active-site region due to their importance in substrate binding and the catalytic mechanism. The RMSD of OXA-48, noncovalently complexed with imipenem, consistently fluctuates below 2 Å throughout the 100 ns MD simulation, and imipenem remains bound to the active site (Figure 8A). The RMSD of OXA-48 complexed with meropenem is consistently lower than 2 Å during the first 60 ns of the simulation and increases during the remainder of the simulation (Figure 8C). At 80 ns, it increases to ~4 Å, and visual inspection reveals that meropenem leaves the active site. The RMSD of OXA-163 complexed with imipenem starts below 2 Å but quickly increases at 10 ns and reaches >6 Å (Figure 8B). Overall, the RMSD has a significant fluctuation ranging between 3 and 6 Å throughout the simulation for the OXA-163/imipenem complex. The imipenem ligand leaves the OXA-163 active site at

approximately 10 ns but does rebind with the protein. The RMSD of the simulation of OXA-163 complexed with meropenem starts at ~2 Å and has a sudden increase at around 25 ns and reaches >5 Å (Figure 8D). The meropenem ligand leaves the OXA-163 active site at 25 ns and stays close to but does not rebind with the protein.

To further investigate the dynamic behavior of OXA-48 and OXA-163 catalytic sites with ligands, the RMSDs of heavy atoms of the active-site amino acids for each simulation are plotted in Figure 9. The RMSD of OXA-48 complexed with imipenem consistently fluctuates around 1 Å throughout the 100 ns MD simulations (Figure 9A). The RMSD of OXA-48 complexed with meropenem fluctuates around 1.5 Å during the 100 ns MD simulations (Figure 9C). The RMSD of the OXA-163 active site when complexed with imipenem fluctuates between 1.5 and 2 Å throughout the simulations (Figure 9B). The RMSD of the OXA-163 active site when complexed with meropenem is the most flexible and has the highest values and largest fluctuation throughout the simulation (Figure 9D).

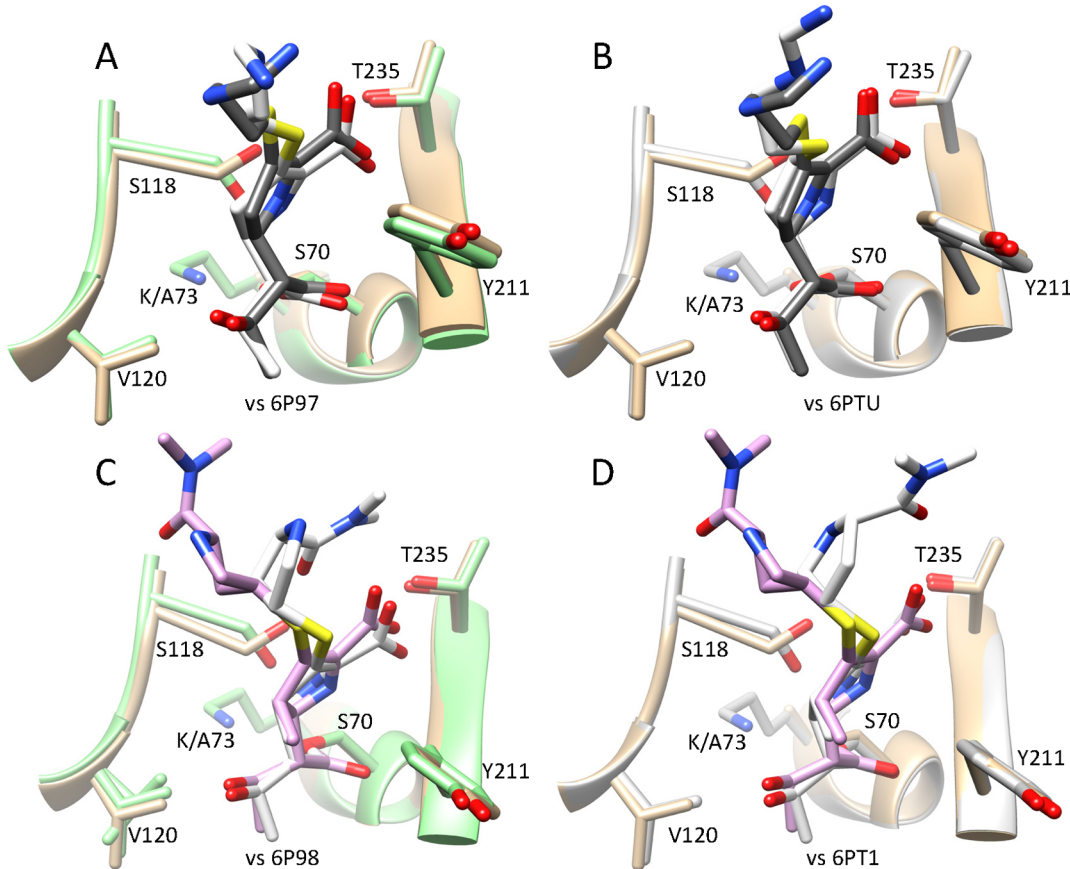


**Figure 6.** X-ray crystal structures of the OXA-48 K73A acyl-enzyme complexes with imipenem and meropenem superimposed with previously determined structures. (A) OXA-48 K73A(tan)/imipenem(gray) aligned with OXA-48(green)/imipenem(white) (PDB ID 6P97). (B) OXA-48 K73A(tan)/imipenem(gray) aligned with OXA-48(white)/imipenem(white) (PDB ID 6PTU). (C) OXA-48 K73A(tan)/meropenem(pink) aligned with OXA-48(green)/meropenem(white) (PDB ID 6P98). (D) OXA-48 K73A(tan)/meropenem(pink) aligned with OXA-48(white)/meropenem(white) (PDB ID 6PT1).

The above analyses suggest, first, that OXA-48 has a more stable binding mode with imipenem than with meropenem and that meropenem (but not imipenem) actually leaves the active site during the simulation. This is consistent with the faster hydrolysis of imipenem compared to that of meropenem by OXA-48 (Table 1). In addition, OXA-48 exhibits more stable binding of both substrates than OXA-163. This is consistent with the finding that OXA-48 catalyzes the hydrolysis of the carbapenems faster than OXA-163 (Table 1). Thus, there is an inverse correlation between the extent of RMSD fluctuation and the rate of catalysis (i.e., a high degree of fluctuation corresponds to slow catalysis). Slow catalysis is therefore associated with the carbapenem substrate and associated active-site residues sampling multiple conformations or substates. If the multiple conformations are largely nonproductive, then the rate of hydrolysis is slower.<sup>49</sup> A caveat is that the MD simulations were performed on the substrate complexes while the rate-determining step for the reactions is deacylation. The strong correlation between the extent of fluctuations observed (RMSD) and the rate of deacylation, however, suggests that the stability of the noncovalent substrate complex is a reflection of the stability of the acyl-enzyme complex.

## DISCUSSION

The OXA-48-like enzymes represent a group with high clinical importance.<sup>19</sup> OXA-48, the first and most widespread member

of OXA-48-like enzymes, is a major contributor to carbapenem resistance among *Klebsiella pneumoniae* infections worldwide and is spreading at an alarming rate.<sup>10</sup> OXA-163 is a natural variant of OXA-48 with a different substrate profile wherein it gains hydrolytic activity against oxyimino-cephalosporins but loses activity toward carbapenems.<sup>26,27</sup> Here we present mechanistic and structural information on the interactions of OXA-48 and OXA-163 enzymes with clinically important carbapenem  $\beta$ -lactam antibiotics imipenem and meropenem. Our detailed kinetic studies show that deacylation is the rate-limiting step in the hydrolysis of carbapenems catalyzed by OXA-48 and OXA-163. Furthermore, the very slow hydrolysis of carbapenems by OXA-163 largely results from specific slowing of the deacylation rate compared to that of OXA-48. Substrate binding and acylation rates are comparable and cannot account for the activity changes. This mechanistic information in combination with the structures of the acyl-enzyme complexes of both enzymes with imipenem and meropenem provides insights into the hydrolysis of carbapenems by the OXA-48 and OXA-163 enzymes.

The OXA-48 enzyme shows higher turnovers of both imipenem and meropenem than OXA-163 due to faster deacylation. Comparisons of the SFC-1 class A carbapenemase versus noncarbapenemase class A enzymes using structural and molecular dynamics data suggest that the hydroxyl group of the  $\alpha$ -hydroxyethyl side chain hydrogen bonds to the deacylation water in noncarbapenemases while in the SFC-1 carbapene-

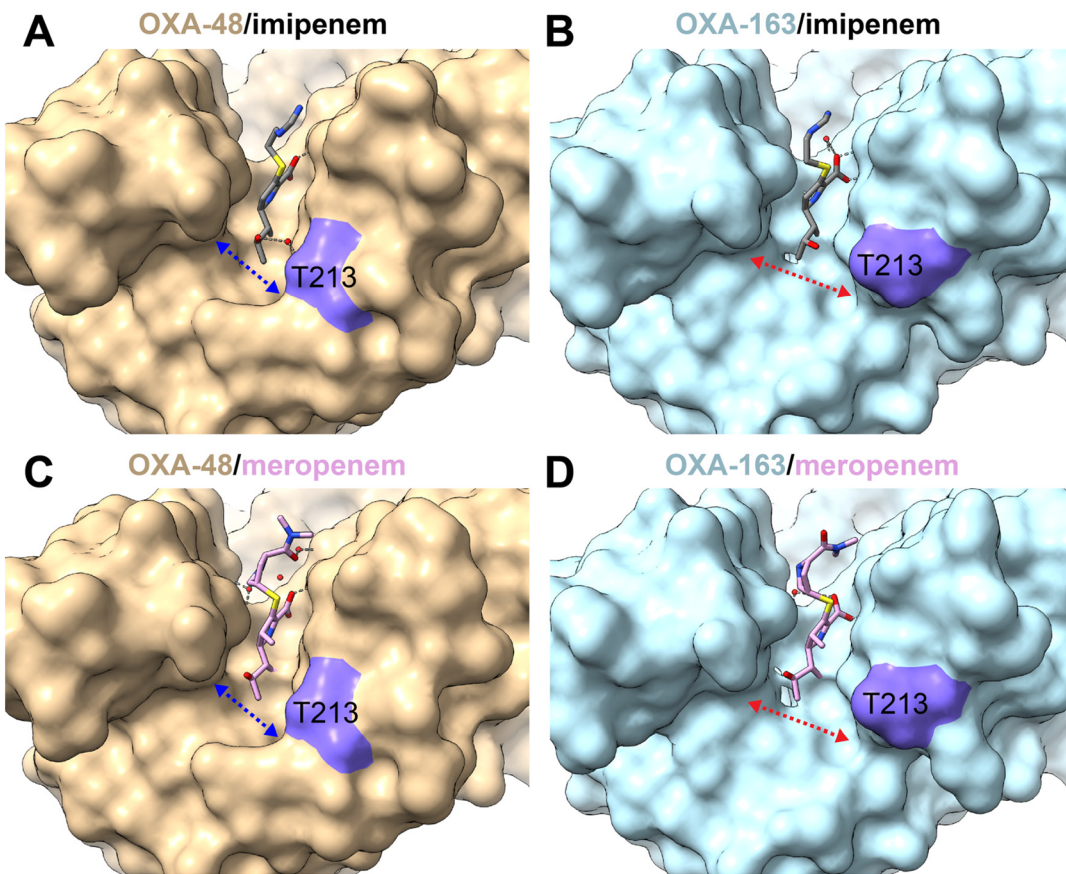


**Figure 7.** Surface representation of the OXA-48 and OXA-163 structures with imipenem and meropenem. (A) OXA-48 structure with acylated imipenem showing the  $\beta 5\text{-}\beta 6$  loop constraint of the active site size near the  $6\alpha$ -hydroxyethyl group. Imipenem carbons are shown in gray, and the OXA-48 surface is shown in tan. The position of Thr213 is shown in purple. The H-bond from Thr213 to the  $6\alpha$ -hydroxyethyl group is through a bridging water molecule. (B) OXA-163 structure with acylated imipenem showing the reduced size of the  $\beta 5\text{-}\beta 6$  loop due to the 214-RIEP-217 deletion that creates a wider active site near the  $6\alpha$ -hydroxyethyl group. The OXA-163 surface is shown in light blue. (C) OXA-48 structure with acylated meropenem showing the constrained region near the  $6\alpha$ -hydroxyethyl group. Meropenem carbons are shown in pink. (D) OXA-163 structure with acylated meropenem showing the wider active site in the region of the  $6\alpha$ -hydroxyethyl group.

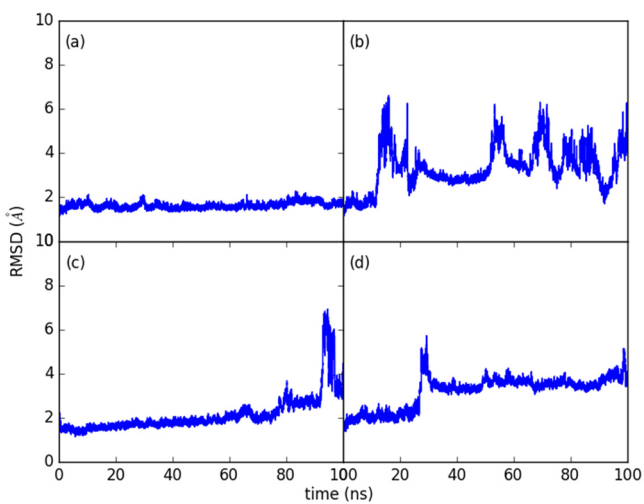


**Figure 8.** RMSD of heavy atoms in the enzyme and substrate complex of four simulations. (a) OXA-48 with imipenem. (b) OXA-163 with imipenem. (c) OXA-48 with meropenem. (d) OXA-163 with meropenem.

mase the hydroxyl group is restrained away from the water.<sup>32</sup> However, the hydroxyl oxygen of the  $6\alpha$ -hydroxyethyl side chain is oriented away from the cavity containing the

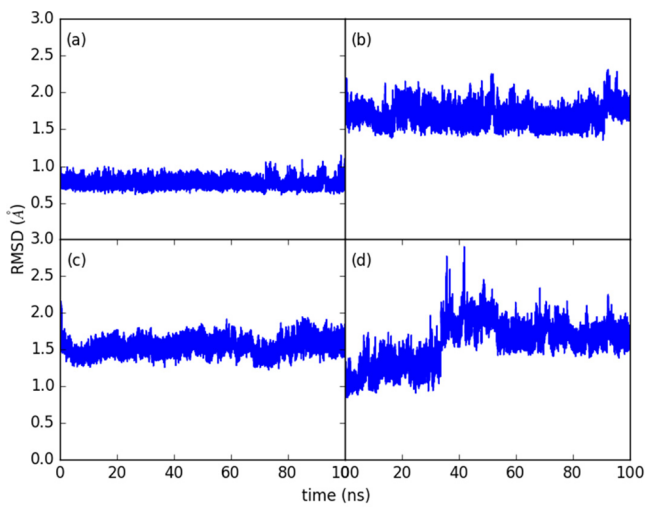


**Figure 9.** RMSD of active-site amino acids of four simulations. (a) OXA-48 with imipenem. (b) OXA-163 with imipenem. (c) OXA-48 with meropenem. (d) OXA-163 with meropenem.

carbamylated Lys73 and deacylation water in both the OXA-48 and OXA-163 structures with imipenem and meropenem, suggesting that this is not the mechanism for the slow reactions

of OXA-163 (Figure 4). Note, however, that the conformations of the hydroxyethyl groups in the structure are similar to those of previous OXA/carbapenemase structures where the Lys73 carbamyl group is missing.<sup>50</sup> Therefore, the position of the hydroxyethyl group observed in our structures may be influenced by the K73A substitution.

An alternate hypothesis that is consistent with the structural results is that the deacylation rate is correlated with the conformational stability of the carbapenem acyl-enzyme intermediate. By this view, the OXA-48 imipenem and meropenem acyl-enzyme intermediates are more stable and sample fewer conformations than the OXA-163 acyl-enzymes. Furthermore, we suggest that a difference in the stability of acylated imipenem and meropenem in the OXA-48 complexes could explain the faster deacylation of imipenem versus meropenem by this enzyme. If the increased stability also applies to the transition state, then it would lead to the observed faster deacylation of imipenem by OXA-48 and the faster deacylation of both imipenem and meropenem by OXA-48 versus OXA-163. We further hypothesize that this effect is more prominent for the OXA-163 carbapenem acyl-enzyme intermediates where the S212D substitution and deletion in the  $\beta$ 5- $\beta$ 6 loop region create a larger active site that does not adequately constrain the carbapenem acyl-enzyme. This results in the intermediate state and the transition state assuming multiple conformations, most of which are inconsistent with rapid deacylation (Figure 6).

Molecular dynamics simulations of the OXA-48 and OXA-163 enzymes in complex with imipenem and meropenem further support the idea that a failure to constrain the conformations of the acyl-enzyme reduces the deacylation rate. We found that OXA-48 has a more stable binding mode with imipenem than with meropenem, which is consistent with the faster hydrolysis of imipenem versus meropenem by OXA-48. Furthermore, OXA-48 exhibits more stable binding of both imipenem and meropenem than OXA-163, which is consistent with the finding that OXA-48 catalyzes the hydrolysis of the carbapenems faster than does OXA-163.

It is also possible that the more open active site of OXA-163 leads to changes in water access to the carbamylated Lys73 general base or the carbonyl carbon of the acyl-enzyme. It has been shown via structural analysis and the molecular dynamics of OXA-48 and OXA-48 with a modified  $\beta$ 5- $\beta$ 6 loop that changes in the loop alter the pathways of water access to the carbamylated Lys73 and carbonyl carbon of the acyl-enzyme.<sup>51,52</sup> In addition, QM/MM simulations of the deacylation reaction for the extended-spectrum cephalosporin ceftazidime suggest that OXA-163 is associated with reduced water access to the carbamylated Lys73 general base, leading to an increased rate of ceftazidime deacylation.<sup>53</sup> Therefore, changes in water access could also contribute to our observed changes in carbapenem deacylation rates.

Previous structural and experimental studies of OXA-48 are consistent with the hypothesis that the  $\beta$ 5- $\beta$ 6 loop region is important to the conformational stability of the carbapenem acyl-enzyme intermediate. On the basis of the structure of OXA-48 and molecular dynamics simulations of a modeled acyl-meropenem intermediate, the unique structure and conformation of the  $\beta$ 5- $\beta$ 6 loop region of OXA-48 are key contributors to its carbapenemase activity.<sup>22</sup> It provides a binding site for the methyl group of the 6 $\alpha$ -hydroxyethyl side chain that results in a conformation allowing water access to the carbonyl carbon for deacylation.<sup>22</sup> An important role for

the  $\beta$ 5- $\beta$ 6 loop is also supported by the gain in carbapenemase activity when the  $\beta$ 5- $\beta$ 6 loop from the carbapenemase, OXA-48 (and OXA-24), is grafted in place of the loop in the noncarbapenemase OXA-10.<sup>54</sup> It was further noted that the PXXG sequence motif found in the C-terminal section of the  $\beta$ 5- $\beta$ 6 loop is found in class D carbapenemases but not in other class D  $\beta$ -lactamases. Our data are consistent with these observations in that OXA-163, which contains a partial deletion of the  $\beta$ 5- $\beta$ 6 loop including the proline from the PXXG sequence, exhibits significantly lower  $k_{cat}$  values for carbapenem hydrolysis than does OXA-48, which has an intact loop. Moreover, the results further indicate that the  $\beta$ 5- $\beta$ 6 loop is important to the efficient deacylation of carbapenem acyl-enzyme intermediates since the lower  $k_{cat}$  values are due to slower deacylation.

Restraining the conformational stability of the enzyme/substrate or enzyme/intermediate complexes has been suggested to be an important aspect of catalytic efficiency and substrate specificity for several systems. For example, conformational stability has been proposed to explain the negative epistasis between TEM-1  $\beta$ -lactamase mutations that extend the substrate specificity to oxyimino-cephalosporins.<sup>49</sup> In this system, individual substitutions increase enzyme conformations that increase active-site access and enhance oxyimino-cephalosporin hydrolysis, but combinations of mutations lead to the disorder and sampling of many unproductive conformations.<sup>49</sup> In addition, directed evolution studies of the LovD enzyme that catalyzes an acyl-transfer reaction showed that the trajectory of evolution toward a new substrate shows changes toward less conformational flexibility that results in enhanced catalytic activity.<sup>55</sup> The results of our mechanistic and structural study of OXA-48 and OXA-163 suggest the restraining conformational flexibility of the carbapenem acyl-enzyme intermediate and the corresponding transition state is an important aspect of class D carbapenemase function.

## METHODS

**Plasmids and Site-Directed Mutagenesis.** The *bla*<sub>OXA-48</sub> and *bla*<sub>OXA-163</sub> protein expression plasmids were constructed by the insertion of the  $\beta$ -lactamase genes into pET29a, as has been described previously.<sup>27</sup> The K73A amino acid substitution was introduced into OXA-48 and OXA-163 by PCR mutagenesis with PfuTurbo DNA Polymerase (Agilent Technologies, Santa Clara, CA, USA) according to the manufacturer's guidelines. DNA sequencing of the entire *bla* gene for each mutant was performed to ensure the absence of extraneous mutations.

**Protein Expression and Purification.** OXA-48 and OXA-163  $\beta$ -lactamases and their respective K73A mutants were expressed in *E. coli* BL21(DE3) cells and purified by affinity and size-exclusion chromatography. In brief, 1L of LB broth containing 30  $\mu$ g/mL kanamycin was inoculated with 10 mL of overnight cell culture and incubated at 37 °C until it reached an OD<sub>600</sub> of 0.6–0.8 before induction with 0.5 mM IPTG. The culture was then grown at 25 °C for 18–20 h with shaking. Cell pellets were obtained by centrifugation at 7000 rpm for 30 min and resuspended in 30 mL of buffer containing 20 mM Tris-HCl pH 8.2 and 20% w/v sucrose. The addition of 60 mL of distilled water with vigorous shaking for 5 min was used to induce periplasmic content release. The resulting spheroblasts were pelleted by centrifugation, and the supernatant was filtered using 0.22  $\mu$ m filters (Corning, NY, USA)

before the addition of 10 mL of 4 M NaCl (400 mM final concentration). The filtrate was loaded onto a fast-flow chelating Sepharose packed column (GE Healthcare, Pittsburgh, PA) charged with zinc. The proteins were eluted with a linear gradient of 150 mM imidazole. The eluted fractions were checked by sodium dodecyl sulfate–polyacrylamide gel electrophoresis (SDS–PAGE). Fractions containing  $\beta$ -lactamases were concentrated using Amicon centrifugal filters with a 10 000 MW cutoff (Merck KGaA, Darmstadt, Germany). After concentration, size-exclusion chromatography using a HiLoad 16/600 Superdex 75 column (GE Healthcare) was performed in 25 mM Tris-HCl (pH 7.7), 25 mM NaCl, and 5 mM NaHCO<sub>3</sub>.  $\beta$ -Lactamase fractions were concentrated, and protein concentrations were determined by absorbance at 280 nm using an extinction coefficient of 63 940 M<sup>-1</sup> cm<sup>-1</sup>.

**Steady-State Kinetics.** Assays were performed on a DU800 spectrophotometer at room temperature (23 °C) in 50 mM NaP<sub>i</sub> buffer (pH 7.2) supplemented with 20 mM NaHCO<sub>3</sub> as previously described.<sup>27</sup>  $\beta$ -Lactam hydrolysis was monitored at wavelengths of 298 nm for meropenem ( $\Delta\epsilon = -7200 \text{ M}^{-1} \text{ cm}^{-1}$ ) and 299 nm for imipenem ( $\Delta\epsilon = -9670 \text{ M}^{-1} \text{ cm}^{-1}$ ). Initial rates were plotted and fit to the Michaelis–Menten equation by nonlinear regression with GraphPad Prism 6 software (GraphPad Software, Inc., La Jolla, CA).

**Acylation Rates ( $k_2$ ) for Carbapenem Hydrolysis.** The linear pathway of  $\beta$ -lactam hydrolysis by serine  $\beta$ -lactamases is outlined in Scheme 1 and consists of two distinct chemical steps (acylation and deacylation) that are associated with rate constants  $k_2$  (acylation) and  $k_3$  (deacylation) (Scheme 1).

The rate constant for the acylation ( $k_2$ ) of carbapenems was determined by pre-steady-state kinetics under single-turnover conditions using a KinTek model SF-2001 stopped-flow apparatus (KinTek Corporation, Clearance, PA).<sup>45</sup> The reactions were performed at 23 °C. Reactions were performed in 50 mM NaP<sub>i</sub> buffer (pH 7.2) supplemented with 20 mM NaHCO<sub>3</sub>. The meropenem reaction was monitored at a wavelength of 298 nm ( $\Delta\epsilon = -7200 \text{ M}^{-1} \text{ cm}^{-1}$ ), and the imipenem reaction was monitored at 299 nm ( $\Delta\epsilon = -9670 \text{ M}^{-1} \text{ cm}^{-1}$ ). The substrate and enzyme were mixed in a 1:1 ratio by volume. The substrate (7.5  $\mu\text{M}$ ) was used with increasing concentrations of enzyme from 10 to 640  $\mu\text{M}$ . For each enzyme concentration, 10–15 measurements were made and averaged. The reaction was followed for 0.1 to 2 s, and the curves were fit to a single-exponential equation (eq 1) to obtain  $k_{\text{obs}}$ . The resulting  $k_{\text{obs}}$  values were fitted with eq 2 where  $K' = (k_{-1} + k_2)/k_1$ .

$$A_t = A_0 e^{-k_{\text{obs}} t} + C \quad (1)$$

$$k_{\text{obs}} = \frac{k_2 [S]}{(K' + [S])} \quad (2)$$

### Deacylation Rates ( $k_3$ ) for Carbapenem Hydrolysis.

Deacylation rates were determined by the reactivation method.<sup>46</sup> Enzymes were incubated with carbapenems at a concentration of at least 10-fold the  $K_m$  value for 0.1–30 min in 50 mM NaP<sub>i</sub> buffer (pH 7.2) supplemented with 20 mM NaHCO<sub>3</sub>. Various incubation times were tested to ensure full recovery of the activity. After incubation, the mixtures were diluted 100- to 200-fold in buffer containing nitrocefin, which was used as a reporter substrate. The final concentration of enzymes was 20 nM for OXA-48 and 30 nM for OXA-163. The final concentration of nitrocefin was 350  $\mu\text{M}$ , which is 10-fold higher than the  $K_m$  for both enzymes. Reactions without

carbapenem incubation were also performed as a control. The reactivation reaction was monitored by nitrocefin hydrolysis at 482 nm ( $\Delta\epsilon = 20\,500 \text{ M}^{-1} \text{ cm}^{-1}$ ). The deacylation rate constants ( $k_3$ ) were determined by fitting the progress curves with eq 3, where  $v_s$  is the velocity of nitrocefin hydrolysis at time  $t$ . It was not possible to measure the  $k_3$  value of OXA-48 for imipenem hydrolysis because of the high  $k_{\text{cat}}$  value. Instead, eq 4 was used to derive  $k_3$  for OXA-48 with imipenem using the experimentally determined values for  $k_2$  and  $k_{\text{cat}}$ . Solving eq 4 for  $k_{\text{cat}}$  in terms of  $k_3$  gives  $k_3 = (k_2 k_{\text{cat}})/(k_{\text{cat}} - k_2)$ . The error in the calculated  $k_3$  value was determined by propagating the errors in  $k_{\text{cat}}$  and  $k_2$  through the equation by adding the absolute errors for the sum (difference) in the denominator to obtain the absolute and the percent errors in  $k_{\text{cat}} - k_2$ . The percent error in the numerator ( $k_{\text{cat}} k_2$ ) was calculated by adding the percent error for  $k_{\text{cat}}$  and  $k_2$ , and the final percent and absolute errors in  $k_3$  were then obtained by adding the percent error of the numerator and denominator to give the percent error in  $k_3$ .

$$A_t = A_0 + v_s t - \frac{v_s}{k_3} (1 - e^{-k_3 t}) \quad (3)$$

$$k_{\text{cat}} = \frac{k_2 k_3}{k_2 + k_3} \quad (4)$$

**Protein Crystallization and Data Collection.** The hanging drop vapor diffusion method was used with a final protein concentration of 5–7 mg/mL in the drop. Crystallization conditions were screened with commercially available screens from Hampton Research (Aliso Viejo, CA) and Qiagen (Venlo, Netherlands) using a 96-well format. Initial crystallization conditions were optimized manually by setting up 24-well plates with a 5  $\mu\text{L}$  final volume of the drops (1:1 protein/well solution). Protein–carbapenem cocrystals were produced under the following conditions: 100 mM Tris-HCl pH 8.5 and 15% PEG 20000 for OXA-48 K73A with imipenem; 220 mM NaCOOH, 3% v/v 2-Methyl-2,4-pentanediol, and 24% PEG 3350 for OXA-163 K73A with imipenem; 200 mM lithium acetate dihydrate and 20% w/w PEG 3350 for OXA-48 K73A with meropenem; and 240 mM NaCOOH, 3% v/v dimethyl sulfoxide, and 22% PEG 3350 for OXA-163 K73A with meropenem. Data sets were collected at beamline 5.0.1 at the Berkeley Center for Structural Biology in the context of the Collaborative Crystallography Program except for OXA-48 with the imipenem data set, which was collected on the home source at Baylor College of Medicine with a Rigaku FR-E SuperBright High-Brilliance Rotating Anode Generator.

### Crystallography Data Processing and Refinement.

Diffraction data were processed using the CCP4 suite.<sup>56</sup> Data were processed using iMOSFLM<sup>57</sup> and scaled and merged with AIMLESS.<sup>58</sup> Structures were determined by molecular replacement with MOLREP<sup>59</sup> using the wild-type structures as search models (OXA-48 PDB ID 3HBR and OXA-163 PDB ID 4S2L). The initial models were refined using REFMAC5<sup>60</sup> and/or PHENIX<sup>61</sup> as implemented in phenix.refine.<sup>62</sup> The models were inspected manually throughout the refinement process using the Crystallography Object-Oriented Toolkit (COOT) program.<sup>63,64</sup> When appropriate, TLS groups were determined using the TLSMD server.<sup>65</sup> The structures were inspected with the PDB REDO server,<sup>66</sup> and final refinement was done using either REFMAC5 or phenix.refine. The final structure was inspected and validated with MolProbity<sup>67</sup> and COOT.<sup>64</sup>

**Programs Used and Structure Coordinates' Deposition.** Structural figures were generated using the UCSF Chimera graphical program.<sup>68</sup> The SSM procedure was used for the superimposition of the structures as implemented in COOT.<sup>64</sup> The atomic coordinates of the structures were deposited in the Protein Data Bank with accession codes 7KH9, 7KHZ, 7KHZ, and 7KHY.

**Molecular Dynamics Simulations.** The crystal structures of OXA-48 and OXA-163 K73A mutants with carbapenem substrates (imipenem and meropenem) and bicarbonate (BCT) were subjected to molecular dynamics (MD) simulations using a molecular mechanics program suite, CHARMM program version 40b1,<sup>69</sup> and the CHARMM36 force field.<sup>70</sup> CHARMM general force fields (CGenFF) for the substrates were generated using the ParamChem online server (<https://cgenff.paramchem.org/>).<sup>71</sup> All systems were solvated in a water box using a TIP3P model<sup>72</sup> with the addition of sodium and chloride ions to balance the charge. The sizes of the simulation boxes are listed in Table S1. The simulation boxes were subjected to 200 steps of the steepest-descent energy minimization and further energy minimization using the adopted basis Newton–Raphson (ABNR) method until the total gradient of the system was lower than 0.03 kcal/mol·Å. Subsequently, the minimized simulation systems were subjected to 12 ps (ps) equilibrium by gradually raising the temperature from 100 to 300 K. The system was then equilibrated via 5 ns (ns) isothermal–isobaric (NTP) ensemble MD simulations at 300 K and 1 atm.

The last frame of the MD simulations was selected, and residue 73 and BCT were modified to lysine Nz-carboxylic acid (Kcx) using CHARMM version 40b1.<sup>69</sup> The modified structures were subjected to energy minimization with steepest descent and ABNR minimization steps. Subsequently, the minimized simulation systems were subjected to 40 ps equilibrium MD simulations by gradually raising the temperature from 100 to 300 K. The system was then subjected to 100 ns NTP ensemble MD simulations at 300 K and 1 atm as production simulations. In all MD simulations, the time step was 2 fs (fs), with all of the bonds associated with hydrogen being fixed during the simulation. Periodic boundary conditions were applied in all simulations. Electrostatic interactions were modeled using the particle mesh Ewald method.<sup>70,73</sup>

The root-mean-square deviation (RMSD) was used to measure the difference in conformation for each snapshot of the MD simulations with regard to the first frame of each simulation. For a molecular structure represented by the Cartesian coordinate vector of  $N$  atoms, the RMSD is calculated as

$$\text{RMSD} = \sqrt{\frac{\sum_{i=1}^N (r_i^0 - Ur_i)^2}{N}} \quad (5)$$

where  $r_i^0$  is the Cartesian coordinate vector for the optimized structure as a reference and  $U$  is the best-fit alignment transformation matrix between a given structure and the reference structure. The RMSD indicates the conformational changes compared to the reference structure. In the system, residues Kcx73, Ser70, Ser118, Trp157, and Lys208 amino acids were defined as the active-site region. The conformational changes in the active site region can influence the substrate binding and catalytic mechanism. Therefore, the RMSD of the heavy atoms of the active-site region and the

RMSD of the heavy atoms of the whole protein plus substrate were calculated.

## ASSOCIATED CONTENT

### SI Supporting Information

The Supporting Information is available free of charge at <https://pubs.acs.org/doi/10.1021/acsinfecdis.0c00798>.

MD simulation cubic box sizes; schematic illustration of the pyrrolidine tautomers associated with carbapenem acyl-enzyme intermediates of  $\beta$ -lactamases; structural alignment of the two molecules in the asymmetric unit of the OXA-48 K73A complex with imipenem; and structural alignment of the two molecules in the asymmetric unit of the OXA-48 K73A complex with imipenem (PDF)

## Accession Codes

The atomic coordinates and structure factors of the OXA-48 and OXA-163 structures have been deposited in the Protein Data Bank under accession codes 7KH9, 7KHZ, 7KHZ, and 7KHY.

## AUTHOR INFORMATION

### Corresponding Author

**Timothy Palzkill** — From the Verna and Marrs McLean Department of Biochemistry and Molecular Biology and Department of Pharmacology and Chemical Biology, Baylor College of Medicine, Houston, Texas 77030, United States;  [orcid.org/0000-0002-5267-0001](https://orcid.org/0000-0002-5267-0001); Phone: (713) 798-5609; Email: [timothyp@bcm.edu](mailto:timothyp@bcm.edu)

### Authors

**Vlatko Stojanoski** — From the Verna and Marrs McLean Department of Biochemistry and Molecular Biology and Department of Pharmacology and Chemical Biology, Baylor College of Medicine, Houston, Texas 77030, United States

**Liya Hu** — From the Verna and Marrs McLean Department of Biochemistry and Molecular Biology, Baylor College of Medicine, Houston, Texas 77030, United States

**Banumathi Sankaran** — Department of Molecular Biophysics and Integrated Bioimaging, Berkeley Center for Structural Biology, Lawrence Berkeley National Laboratory, Berkeley, California 94720, United States

**Feng Wang** — Department of Chemistry, Center for Research Computing, Center for Drug Discovery, Design, and Delivery (CD4), Southern Methodist University, Dallas, Texas 75205, United States;  [orcid.org/0000-0001-7808-7538](https://orcid.org/0000-0001-7808-7538)

**Peng Tao** — Department of Chemistry, Center for Research Computing, Center for Drug Discovery, Design, and Delivery (CD4), Southern Methodist University, Dallas, Texas 75205, United States

**B. V. Venkataram Prasad** — From the Verna and Marrs McLean Department of Biochemistry and Molecular Biology, Baylor College of Medicine, Houston, Texas 77030, United States

Complete contact information is available at:  
<https://pubs.acs.org/10.1021/acsinfecdis.0c00798>

### Funding

This work was supported by NIH grant R01 AI32956 to T.P., Welch Foundation grant Q1279 to B.V.V.P., and NSF CAREER grant 1753167 to P.T. The ALS-ENABLE beamlines are supported in part by the National Institutes of Health,

National Institute of General Medical Sciences, grant P30 GM124169-01. The Advanced Light Source is a Department of Energy Office of Science User Facility under contract no. DE-AC02-05CH11231. Computational time was provided by the Southern Methodist University's Center for Research Computing.

## Notes

The authors declare no competing financial interest.

## ACKNOWLEDGMENTS

The authors thank Dr. Hiram Gilbert for comments on the manuscript.

## REFERENCES

- (1) Martens, E., and Demain, A. L. (2017) The antibiotic resistance crisis, with a focus on the United States. *J. Antibiot.* 70, 520–526.
- (2) Holmes, A. H., Moore, L. S. P., Sundsfjord, A., Steinbakk, M., Regmi, S., Karkey, A., Guerin, P. J., and Piddock, L. J. V. (2016) Understanding the mechanisms and drivers of antimicrobial resistance. *Lancet* 387, 176–187.
- (3) Nordmann, P., Cuzon, G., and Naas, T. (2009) The real threat of *Klebsiella pneumoniae* carbapenemase-producing bacteria. *Lancet Infect. Dis.* 9, 228–236.
- (4) Nordmann, P., Dortet, L., and Poirel, L. (2012) Carbapenem resistance in Enterobacteriaceae: here is the storm. *Trends Mol. Med.* 18, 263–272.
- (5) Guh, A. Y., Bulens, S. N., Mu, Y., Jacob, J. T., Reno, J., Scott, J., Wilson, L. E., Vaeth, E., Lynfield, R., Shaw, K. M., Vagnone, P. M. S., Bamberg, W. M., Janelle, S. J., Dumyati, G., Concannon, C., Beldavs, Z., Cunningham, M., Cassidy, P. M., Phipps, E. C., Kenslow, N., Travis, T., Lonsway, D., Rasheed, J. K., Limbago, B. M., and Kallen, A. J. (2015) Epidemiology of Carbapenem-Resistant Enterobacteriaceae in 7 US Communities, 2012–2013. *JAMA* 314, 1479–1487.
- (6) Poirel, L., Pitout, J. D., and Nordmann, P. (2007) Carbapenemases: molecular diversity and clinical consequences. *Future Microbiol.* 2, 501–512.
- (7) Paterson, D. L. (2006) Resistance in gram-negative bacteria: Enterobacteriaceae. *Am. J. Infect. Control* 34, S20–S28 discussion S64–S73.
- (8) Garbati, M. A., and Al Godhair, A. I. (2013) The growing resistance of *Klebsiella pneumoniae*; the need to expand our antibiogram: case report and review of the literature. *Afr. J. Infect. Dis.* 7, 8–10.
- (9) Broberg, C. A., Palacios, M., and Miller, V. L. (2014) Klebsiella: a long way to go towards understanding this enigmatic jet-setter. *F1000Prime Rep.* 6, 64.
- (10) Pitout, J. D. D., Nordmann, P., and Poirel, L. (2015) Carbapenemase-producing *Klebsiella pneumoniae*, a key pathogen set for global nosocomial Dominance. *Antimicrob. Agents Chemother.* 59, 5873–5884.
- (11) Nicolau, D. P. (2008) Carbapenems: a potent class of antibiotics. *Expert Opin. Pharmacother.* 9, 23–37.
- (12) Papp-Wallace, K. M., Endimiani, A., Taracila, M. A., and Bonomo, R. A. (2011) Carbapenems: past, present, and future. *Antimicrob. Agents Chemother.* 55, 4943–4960.
- (13) McKenna, M. (2013) Antibiotic resistance: the last resort. *Nature* 499, 394–396.
- (14) Rapp, R. P., and Urban, C. (2012) *Klebsiella pneumoniae* carbapenemases in Enterobacteriaceae: history, evolution, and microbiology concerns. *Pharmacother.* 32, 399–407.
- (15) Tang, S. S., Apisarnthanarak, A., and Hsu, L. Y. (2014) Mechanisms of  $\beta$ -lactam antimicrobial resistance and epidemiology of major community- and healthcare-associated multidrug-resistant bacteria. *Adv. Drug Delivery Rev.* 78, 3–13.
- (16) Bush, K., and Jacoby, G. A. (2010) Updated functional classification of beta-lactamases. *Antimicrob. Agents Chemother.* 54, 969–976.
- (17) Ambler, R. P. (1980) The structure of beta-lactamases. *Philos. Trans. R. Soc. London, Ser. B* 289, 321–331.
- (18) Nordmann, P., Naas, T., and Poirel, L. (2011) Global spread of Carbapenemase-producing Enterobacteriaceae. *Emerging Infect. Dis.* 17, 1791–1798.
- (19) Poirel, L., Potron, A., and Nordmann, P. (2012) OXA-48-like carbapenemases, the phantom menace. *J. Antimicrob. Chemother.* 67, 1597–1606.
- (20) Nordmann, P., Poirel, L., Walsh, T. R., and Livermore, D. M. (2011) The emerging NDM carbapenemases. *Trends Microbiol.* 19, 588–595.
- (21) Poirel, L., Héritier, C., Tolün, V., and Nordmann, P. (2004) Emergence of oxacillinase-mediated resistance to imipenem in *Klebsiella pneumoniae*. *Antimicrob. Agents Chemother.* 48, 15–22.
- (22) Docquier, J.-D., Calderone, V., De Luca, F., Benvenuti, M., Giuliani, F., Bellucci, L., Tafi, A., Nordmann, P., Botta, M., Rossolini, G. M., and Mangani, S. (2009) Crystal structure of the OXA-48 beta-lactamase reveals mechanistic diversity among class D carbapenemases. *Chem. Biol.* 16, 540–547.
- (23) Dortet, L., Oueslati, S., Jeannot, K., Tandé, D., Naas, T., and Nordmann, P. (2015) Genetic and biochemical characterization of OXA-405, an OXA-48-type extended-spectrum  $\beta$ -lactamase without significant carbapenemase activity. *Antimicrob. Agents Chemother.* 59, 3823–3828.
- (24) Oueslati, S., Nordmann, P., and Poirel, L. (2015) Heterogeneous hydrolytic features for OXA-48-like  $\beta$ -lactamases. *J. Antimicrob. Chemother.* 70, 1059–1063.
- (25) Gomez, S., Pasteran, F., Faccione, D., Bettoli, M., Veliz, O., De Belder, D., Rapoport, M., Gatti, B., Petroni, A., and Corso, A. (2013) Intrapatient emergence of OXA-247: a novel carbapenemase found in a patient previously infected with OXA-163-producing *Klebsiella pneumoniae*. *Clin. Microbiol. Infect.* 19, E233–E235.
- (26) Poirel, L., Castanheira, M., Carrér, A., Rodriguez, C. P., Jones, R. N., Smayevsky, J., and Nordmann, P. (2011) OXA-163, an OXA-48-related class D  $\beta$ -lactamase with extended activity toward expanded-spectrum cephalosporins. *Antimicrob. Agents Chemother.* 55, 2546–51.
- (27) Stojanoski, V., Chow, D.-C., Fryszczyn, B., Hu, L., Nordmann, P., Poirel, L., Sankaran, B., Prasad, B. V. V., and Palzkill, T. (2015) Structural basis for different substrate profiles of two closely related Class D  $\beta$ -Lactamases and their inhibition by halogens. *Biochemistry* 54, 3370–3380.
- (28) Golemi, D., Maveyraud, L., Vakulenko, S., Tranier, S., Ishiwata, A., Kotra, L. P., Samama, J.-P., and Mobashery, S. (2000) The first structural and mechanistic insights for class D  $\beta$ -lactamases: Evidence for a novel catalytic process for turnover of  $\beta$ -lactam antibiotics. *J. Am. Chem. Soc.* 122, 6132–6133.
- (29) Golemi, D., Maveyraud, L., Vakulenko, S., Samama, J. P., and Mobashery, S. (2001) Critical involvement of a carbamylated lysine in catalytic function of class D beta-lactamases. *Proc. Natl. Acad. Sci. U. S. A.* 98, 14280–14285.
- (30) Maveyraud, L., Mourey, L., Kotra, L. P., Pedelacq, J.-D., Guillet, V., Mobashery, S., and Samama, J.-P. (1998) Structural basis for clinical longevity of carbapenem antibiotics in the face of challenge by the common class A  $\beta$ -Lactamases from the antibiotic-resistant bacteria. *J. Am. Chem. Soc.* 120, 9748–9752.
- (31) Nukaga, M., Bethel, C. R., Thomson, J. M., Hujer, A. M., Distler, A., Anderson, V. E., Knox, J. R., and Bonomo, R. A. (2008) Inhibition of class A  $\alpha$ -lactamases by carbapenems: Crystallographic observation of two conformations of Meropenem in SHV-1. *J. Am. Chem. Soc.* 130, 12656–12662.
- (32) Fonseca, F., Chudyk, E. I., van der Kamp, M. W., Correia, A., Mulholland, A. J., and Spencer, J. (2012) The basis for carbapenem hydrolysis by class A  $\beta$ -lactamases: A combined investigation using crystallography and simulations. *J. Am. Chem. Soc.* 134, 18275–18285.
- (33) Tremblay, L. W., Fan, F., and Blanchard, J. S. (2010) Biochemical and structural characterization of *Mycobacterium tuberculosis*  $\beta$ -lactamase with the carbapenems ertapenem and doripenem. *Biochemistry* 49, 3766–3773.

- (34) Kalp, M., and Carey, P. R. (2008) Carbapenems and SHV-1 beta-lactamase form different acyl-enzyme populations in crystals and solution. *Biochemistry* 47, 11830–11837.
- (35) Toth, M., Smith, C. A., Antunes, N. T., Stewart, N. K., Maltz, L., and Vakulenko, S. B. (2017) The role of conserved surface hydrophobic residues in the carbapenemase activity of the class D  $\beta$ -lactamases. *Acta Crystallogr. D Struct Biol.* 73, 692–701.
- (36) Akhtar, A., Pemberton, O. A., and Chen, Y. (2020) Structural basis for substrate specificity and carbapenemase activity of OXA-48 Class D  $\beta$ -Lactamase. *ACS Infect. Dis.* 6, 261–271.
- (37) Akhter, S., Lund, B. A., Ismael, A., Langer, M., Isaksson, J., Christopeit, T., Leiros, H.-K. S., and Bayer, A. (2018) A focused fragment library targeting the antibiotic resistance enzyme - Oxacillinase-48: Synthesis, structural evaluation and inhibitor design. *Eur. J. Med. Chem.* 145, 634–648.
- (38) Smith, C. A., Stewart, N. K., Toth, M., and Vakulenko, S. B. Structural insights into the mechanism of carbapenemase activity of the OXA-48  $\beta$ -Lactamase. *Antimicrob. Agents Chemother.* 2019, 63, DOI: 10.1128/AAC.01202-19.
- (39) Héritier, C., Poirel, L., Aubert, D., and Nordmann, P. (2003) Genetic and functional analysis of the chromosome-encoded carbapenem-hydrolyzing oxacillinase OXA-40 of *Acinetobacter baumannii*. *Antimicrob. Agents Chemother.* 47, 268–273.
- (40) Walther-Rasmussen, J., and Høiby, N. (2006) OXA-type carbapenemases. *J. Antimicrob. Chemother.* 57, 373–383.
- (41) Galleni, M., and Frere, J.-M. (2007) Kinetics of  $\beta$ -lactamases and penicillin-binding proteins. In *Enzyme-Mediated Resistance to Antibiotics: Mechanisms, Dissemination, and Prospects for Inhibition*; Bonomo, R. A., and Tolmasky, M. E., Eds.; ASM Press: Washington, D.C., pp 67–79.
- (42) Palzkill, T. (2018) Structural and mechanistic basis for extended-spectrum drug-resistance mutations in altering the specificity of TEM, CTX-M, and KPC,  $\beta$ -lactamases. *Front. Mol. Biosci.* 5, 16.
- (43) Frase, H., Shi, Q., Testero, S. A., Mobashery, S., and Vakulenko, S. B. (2009) Mechanistic basis for the emergence of catalytic competence against carbapenem antibiotics by the GES family of beta-lactamases. *J. Biol. Chem.* 284, 29509–29513.
- (44) Christensen, H., Martin, M., and Waley, G. (1990) Beta-Lactamases as fully efficient enzymes. *Biochem. J.* 266, 853–861.
- (45) Bicknell, R., and Waley, S. G. (1985) Single-turnover and steady-state kinetics of hydrolysis of cephalosporins by beta-lactamase I from *Bacillus cereus*. *Biochem. J.* 231, 83–88.
- (46) Koerber, S. C., and Fink, A. L. (1987) The analysis of enzyme progress curves by numerical differentiation, including competitive product inhibition and enzyme reactivation. *Anal. Biochem.* 165, 75–87.
- (47) Hollaway, M. R., Antonini, E., and Brunori, M. (1969) The ficin-catalysed hydrolysis of p-nitrophenyl hippurate. Detailed kinetics including the measurement of the apparent dissociation constant for the enzyme-substrate complex. *FEBS Lett.* 4, 299–306.
- (48) June, C. M., Vallier, B. C., Bonomo, R. A., Leonard, D. A., and Powers, R. A. (2014) Structural origins of oxacillinase specificity in class D  $\beta$ -lactamases. *Antimicrob. Agents Chemother.* 58, 333–341.
- (49) Dellus-Gur, E., Elias, M., Caselli, E., Prati, F., Salverda, M. L., de Visser, J. A., Fraser, J. S., and Tawfik, D. S. (2015) Negative epistasis and evolvability in TEM-1 -lactamase—The thin line between and enzyme's conformational freedom and disorder. *J. Mol. Biol.* 427, 2396–2409.
- (50) Aertker, K. M. J., Chan, H. T. H., Lohans, C. T., and Schofield, C. J. (2020) Analysis of  $\beta$ -lactone formation by clinically observed carbapenemases informs on a novel antibiotic resistance mechanism. *J. Biol. Chem.* 295, 16604–16613.
- (51) Oueslati, S., Retailleau, P., Marchini, L., Berthault, C., Doret, L., Bonnin, R. A., Iorga, B. I., and Naas, T. Role of arginine 214 in the substrate specificity of OXA-48. *Antimicrob. Agents Chemother.* 2020, 64.
- (52) Dabos, L., Zavala, A., Bonnin, R. A., Beckstein, O., Retailleau, P., Iorga, B. I., and Naas, T. (2020) Substrate specificity of OXA-48 after  $\beta$ S- $\beta$ 6 loop replacement. *ACS Infect. Dis.* 6, 1032–1043.
- (53) Hirvonen, V. H. A., Mulholland, A. J., Spencer, J., and van der Kamp, M. W. (2020) Small changes in hydration determine cephalosporinase activity of OXA-48  $\beta$ -lactamases. *ACS Catal.* 10, 6188–6196.
- (54) De Luca, F., Benvenuti, M., Carboni, F., Pozzi, C., Rossolini, G. M., Mangani, S., and Docquier, J.-D. (2011) Evolution to carbapenem-hydrolyzing activity in noncarbapenemase class D  $\beta$ -lactamase OXA-10 by rational protein design. *Proc. Natl. Acad. Sci. U. S. A.* 108, 18424–18429.
- (55) Jiménez-Osés, G., Osuna, S., Gao, X., Sawaya, M. R., Gilson, L., Collier, S. J., Huisman, G. W., Yeates, T. O., Tang, Y., and Houk, K. N. (2014) The role of distant mutations and allosteric regulation on LovD active site dynamics. *Nat. Chem. Biol.* 10, 431–436.
- (56) Winn, M. D., Ballard, C. C., Cowtan, K. D., Dodson, E. J., Emsley, P., Evans, P. R., Keegan, R. M., Krissinel, E. B., Leslie, A. G., McCoy, A., McNicholas, S. J., Murshudov, G. N., Pannu, N. S., Potterton, E. A., Powell, H. R., Read, R. J., Vagin, A., and Wilson, K. S. (2011) Overview of the CCP4 suite and current developments. *Acta Crystallogr., Sect. D: Biol. Crystallogr.* 67, 235–242.
- (57) Battye, T. G., Kontogiannis, L., Johnson, O., Powell, H. R., and Leslie, A. G. (2011) iMOSFLM: a new graphical interface for diffraction-image processing with MOSFLM. *Acta Crystallogr., Sect. D: Biol. Crystallogr.* 67, 271–281.
- (58) Evans, P. R., and Murshudov, G. N. (2013) How good are my data and what is the resolution? *Acta Crystallogr., Sect. D: Biol. Crystallogr.* 69, 1204–1214.
- (59) Vagin, A., and Teplyakov, A. (2010) Molecular replacement with MOLREP. *Acta Crystallogr., Sect. D: Biol. Crystallogr.* 66, 22–25.
- (60) Vagin, A. A., Steiner, R. A., Lebedev, A. A., Potterton, L., McNicholas, S., Long, F., and Murshudov, G. N. (2004) REFMACS dictionary: organization of prior chemical knowledge and guidelines for its use. *Acta Crystallogr., Sect. D: Biol. Crystallogr.* 60, 2184–2195.
- (61) Adams, P. D., Afonine, P. V., Bunkoczi, G., Chen, V. B., Davis, I. W., Echols, N., Headd, J. J., Hung, L. W., Kapral, G. J., Gross-Kunstleve, R. W., McCoy, A. J., Moriarty, N. W., Oeffner, R., Read, R. J., Richardson, D. C., Richardson, J. S., Terwilliger, T. C., and Zwart, P. H. (2010) PHENIX: a comprehensive Python-based system for macromolecular structure solution. *Acta Crystallogr., Sect. D: Biol. Crystallogr.* 66, 213–21.
- (62) Liebschner, D., Afonine, P. V., Baker, M. L., Bunkóczki, G., Chen, V. B., Croll, T. I., Hintze, B., Hung, L. W., Jain, S., McCoy, A. J., Moriarty, N. W., Oeffner, R. D., Poon, B. K., Prisant, M. G., Read, R. J., Richardson, J. S., Richardson, D. C., Sammito, M. D., Sobolev, O. V., Stockwell, D. H., Terwilliger, T. C., Urzhumtsev, A. G., Videau, L. L., Williams, C. J., and Adams, P. D. (2019) Macromolecular structure determination using X-rays, neutrons and electrons: recent developments in Phenix. *Acta Crystallogr. D Struct. Biol.* 75, 861–877.
- (63) Emsley, P., and Cowtan, K. (2004) Coot: model-building tools for molecular graphics. *Acta Crystallogr., Sect. D: Biol. Crystallogr.* 60, 2126–2132.
- (64) Emsley, P., Lohkamp, B., Scott, W. G., and Cowtan, K. (2010) Features and development of Coot. *Acta Crystallogr., Sect. D: Biol. Crystallogr.* 66, 486–501.
- (65) Painter, J., and Merritt, E. A. (2006) Optimal description of a protein structure in terms of multiple groups undergoing TLS motion. *Acta Crystallogr., Sect. D: Biol. Crystallogr.* 62, 439–450.
- (66) Joosten, R. P., Long, F., Murshudov, G. N., and Perrakis, A. (2014) The PDB\_REDQ server for macromolecular structure model optimization. *IUCrJ* 1, 213–220.
- (67) Chen, V. B., Arendall, W. B., Headd, J. J., Keedy, D. A., Immormino, R. M., Kapral, G. J., Murray, L. W., Richardson, J. S., and Richardson, D. C. (2010) MolProbity: all-atom structure validation for macromolecular crystallography. *Acta Crystallogr., Sect. D: Biol. Crystallogr.* 66, 12–21.
- (68) Pettersen, E. F., Goddard, T. D., Huang, C. C., Couch, G. S., Greenblatt, D. M., Meng, E. C., and Ferrin, T. E. (2004) UCSF Chimera—a visualization system for exploratory research and analysis. *J. Comput. Chem.* 25, 1605–1612.

(69) Halgren, T. (1992) The representation of van der Waals (vdW) interactions in molecular mechanics force fields: potential form, combination rules, and vdW parameters. *J. Am. Chem. Soc.* 114, 7827–7843.

(70) Best, R. B., Zhu, X., Shim, J., Lopes, P. E. M., Mittal, J., Feig, M., and Mackerell, A. D. (2012) Optimization of the additive CHARMM all-atom protein force field targeting improved sampling of the backbone  $\varphi$ ,  $\psi$  and side-chain  $\chi(1)$  and  $\chi(2)$  dihedral angles. *J. Chem. Theory Comput.* 8, 3257–3273.

(71) Vanommeslaeghe, K., Hatcher, E., Acharya, C., Kundu, S., Zhong, S., Shim, J., Darian, E., Guvench, O., Lopes, P., Vorobyov, I., and Mackerell, A. D. (2010) CHARMM general force field: A force field for drug-like molecules compatible with the CHARMM all-atom additive biological force fields. *J. Comput. Chem.* 31, 671–690.

(72) Jorgensen, W. L., Chandrasekhar, J., Madura, J. D., Impey, R. W., and Klein, M. L. (1983) Comparison of simple potential functions for simulating liquid water. *J. Chem. Phys.* 79, 926–935.

(73) Brooks, B. R., Brooks, C. L., Mackerell, A. D., Nilsson, L., Petrella, R. J., Roux, B., Won, Y., Archontis, G., Bartels, C., Boresch, S., Caflisch, A., Caves, L., Cui, Q., Dinner, A. R., Feig, M., Fischer, S., Gao, J., Hodoscek, M., Im, W., Kuczera, K., Lazaridis, T., Ma, J., Ovchinnikov, V., Paci, E., Pastor, R. W., Post, C. B., Pu, J. Z., Schaefer, M., Tidor, B., Venable, R. M., Woodcock, H. L., Wu, X., Yang, W., York, D. M., and Karplus, M. (2009) CHARMM: the biomolecular simulation program. *J. Comput. Chem.* 30, 1545–1614.